CHAPTER I

INTRODUCTION

1.1 Background and rationale

Sandstone formations shape landscapes worldwide, but their susceptibility to erosion process is challenging for engineering works, for examples slope embankments, dams, and reservoirs. In northeast of Thailand, sandstones are layering deposited, where Phu Phan and Phra Wihan formations host a variety of infrastructures and constructions within the area. To understand the erosion process, several investigators attempt to study the governing factors and forecast their behaviors in long-term conditions (Jamshidi, 2023; Moradian, Ghazvinian, Ahmadi, & Behnia, 2010; Xiang, Latham, & Pain, 2022). The complexity of field factors limit the ability to isolate internal factors and specific mechanisms, while laboratory simulations offer a controlled environment to accelerate the process, examine specific factors, and develop a deeper understanding of the erosion dynamics for sandstones. The relative importance of these factors can be correlated to predict the potential behaviors of rocks. Nichols (2009) reports that the resistance to this process can be described in terms of durability parameters. One of the prevalent methods is slake durability index [SDI] tests, as specified by the American Society for Testing and Materials [ASTM], (ASTM D4644, 2016). The determination and classification for this index have widely been developed to correlate the degradation degrees between rocks (e.g. Ergular & Shakoor, 2009; Franklin & Chandra, 1972; Moradian et al., 2010; Zhu & Deng, 2019). However, recent studies concentrated using this method for rock durability only in terms of physical weathering process. To develop this technique for erosion process. The movement of rocks and transport velocity are concerned with the estimation of consumption energy during erosion process. The mathematical representation correlating between degrees of erosion and the required energy is developed. This study would be useful as one of the technique to apply for long-term prediction of rock erosion with the correlation parameters under laboratory simulation. The assessment of the energy consumption for rock erosion can be useful for further understand of rock degradtion behaviors in the selective area.

1.2 Research objectives

The objective of this study is to simulate the effect of erosion process on three Thai sandstones. The main task involves performing slake durability index test under dry and wet conditions. Test parameters are increasing up to 2,000 revolutions for 80 cycles beyond the ASTM D4644-16 standard specifications to obtain results that can represent long-term durability of rock specimens. Mineralogical and physical characteristics of the specimens are considered in the analysis. The specimens durability is correlated with the energy required to induce different degrees of degradation, and hence allows predicting long-term erosion process for the rocks.

1.3 Scope and Limitations

The scope and limitations of the study include as follows:

1) Slake durability test will be performed on cubic specimens, prepared from Phu Phan conglomeratic sandstone, Phu Phan and Phra Wihan sandstones.
2) The nominal mass for cubic specimens are 50±5 g.
3) Slake durability tests procedure will be modified from ASTM D4644-16 standard by performing from 200 to 2,000 revolution and increasing up to 80 test cycles (days) for each rock specimens.
4) The tests will be performed under wet and dry conditions with controlled of ambient temperature for 25±2 °C.
5) The oven-dry setting are controlled with 105±5 °C for 20 hours.

6) Weight measurement is analyzed before testing in each test cycle to determine mass balance.

7) Surface observation and physical measurements are analyzed every 20 cycles.

8) Rock fragments before and after test through 80 cycles are analyzed mineral compositions.

9) Passing materials from the drums are collected after each test cycle for all conditions and analyzed mineral compositions using X-ray diffraction analysis.

1.4 Research methodology

The research methodology shown in Figure 1.1 comprises six steps: including literature reviews, sample collecting and preparation, slake durability test and physical measurements, test results and analysis, energy analysis, discussions, conclusions, and thesis writing.

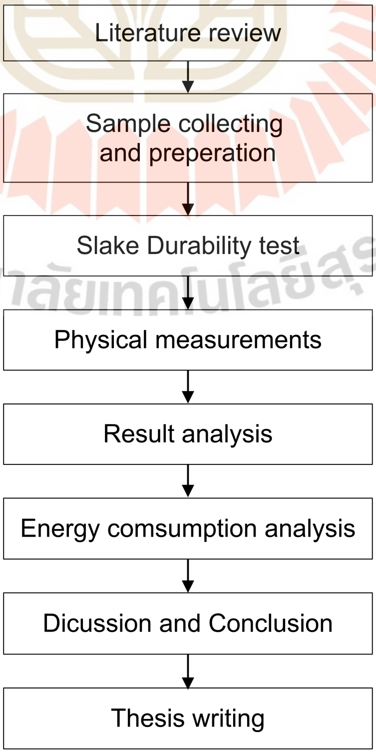

Figure 1.1 Research methodolody

1.4.1 Literature review

Literature review will be performed to enhance the understanding of terms and definitions for erosion and related processes. This section also include with developed techniques reflecting the degradations through rocks durability and their energy consumption. The reviwed for relative of erosional factors under field and laboratory conditions will be conducted to explain mechanisms for erosional process. The erosional factors due to mineralogical and physical characteristics on previous researches are determined for better understanding of rock erosion behaviors.

1.4.2 Sample collecting and preparation

Rock samples are collected from northeast of Thailand. Phra Wihan sandstone and conglomeratic and bedded sandstones from Phu Phan formation are selected for this study. Each rock type is prepared into cubic shape. Twenty specimens are setted for each condition with an average mass of 50 g. The nominal dimension of initial fragments had approximate axes of 27.5 mm^3.

1.4.3 Slake durability test

The slake durability is tested follows the suggestion of ASTM D4644-16 standard (ASTM, 2016). The tests are modified from the standard by performed 2,000 revolutions, instead of 200 revolutions and incresed test cycles up to 80 from 2 cycles. Each set of ten cubical fragments are subjecting to dry and wet conditions. After each test cycle, fragments are heated with 105 ± 5 °C over 20 hours. Before testing in the next cycle, each fragment is cooled down at ambient temperature for 1 hour and weight measurement. Surface observations are analyzed with an interval of 20 test cycles. The particles passing through the drums are collected for X-ray diffraction (XRD) analysis.

1.4.4 Physical measurements

Physical properties include: density, shape, and size are measured for every 20 test cycles. For density, the measurement is conducted as suggested by ASTM D7263-21 standard test method. Variation of shapes and sizes determination follows the method from Hryciw et al. (2016). The mineral contents for fragments from each rock type are analyzed before and after test through 80 cycles. The passing materials are also collected for mineral analysis.

1.4.5 Results analysis

The physical properties are correlated to conduct the characteristics of each rock under dry and wet conditions. The mineral compositions of fragments before and after 80 test cycles wil be analyzed as a volumatic weight percents for calcuclated porosity. The analysis will be followed the method of Chamwon, Thongpprapha, and Fuenkajorn (2020), where the results comparing to those obtained from ASTM D7263-21 (ASTM,2021) standard test method. The passing materials from slake durability tests under both conditions are analyzed as the accumerative passing weight percents for further analysis of required energy for rock degradations.

1.4.6 Energy consumption analysis

The mathematical relationship is represented the degradation energy for rocks from each test cycle. The results are expressed to establish the rock erosion prediction. Energy assessments according to the statistical analysis is further applied for each rock with its fragments size.

1.4.7 Discussions and Conclusions

Discussions and conclusions in this study will make on the reliability and adequacies of the approaches used to determine the resulting relationship. The thesis will include research activities, methods, and results. The research or results will be published in conference proceedings or journals.

1.4.8 Thesis writing

All research activities, methods, and results will be documented and complied in the thesis. The findings will be published in conference proceedings or journals.

1.5 Thesis content

The contents are presented through eight chapters. Chapter I introduces the background, objectives, scope, limitations, and briefly method uses in this study. Chapter II summarizes previous researches including definitions and terms of erosion process with previous simulation techniques, erosional factors, and energy involving in environmental systems. Chapter III describes collecting area, sample preparation and physical properties for PWSS, PPCS, and PPSS specimens before testing. Chapter IV explains test methods for slake durability test and physical measurements. Chapter V shows test results. Chapter VI offers the analysis for physical properties and the passing materials from slake durability tests. Chapter VII represents energy using for three rocks to disintgrate and their applications. Chapter VIII discusses and concludes the obtained results. Future studies are recommended for further knowledge that should be concerned.

CHAPTER II

LITERATURE REVIEW

This chapter summarizes findings from previous research studies to enhance an understanding of the relationship between slake durability tests, erosional process, and related energy. The following contents are an overview of related topics, including (1) rock erosion process, (2) simulation of erosion and slake durability test, (3) erosional factors, and (4) erosive energy.

2.1 Rock erosion process

Erosion is one of the processes that governing the degradation behavior of rock. This process occurs through various mechanisms. It requires dynamic force within rock itself to cause the detachment (physical weathering) and the external forces to transport in an environment systems (Krautblatter & Moore, 2014; Paripuri, Parian, & Rosenkranz, 2020). Foye (1921) delineates two different mechanisms in the process: (1) mechanical erosion (corrasion) and (2) chemical erosion (corrosion). These mechanisms work in a similar way in the weathering process. Only the mechanical erosion requires motion of atmospheric action, and chemical erosion occurs to alter the internal components within rocks though action of chemical agents that present in the transporting environments.

2.2 Simulation of erosion and slake durability test

For simulating erosion, the laboratory and numerical models are extensively used by researchers to understand the impact of degradation process under severe conditions. Variety of techniques are employed to replicate the complex behaviors under wind and water, with the isolated and controllable of specific conditions through simulation, it tend to provide specific factors that governing degradation corresponds to variation of rock types. Some of them are simulated by setting the external forces, including plunge pool, water and aerial jets (George & Sitar, 2012; Scheingross & Lamb, 2017; Xiang, Latham, & Pain, 2022). Figure 2.1 shows the schematic of plunge pool technique.

According to the state reviews of Moses, Robinson, and Barlow (2014). Several researchers are precisely calibrated the laboratory and numerical simulation results against field data to reflect each rock in the environmental systems. Summarization of related techniques are shown in Table 2.1. The results and erosional factors from these techniques will be stated in the following section.

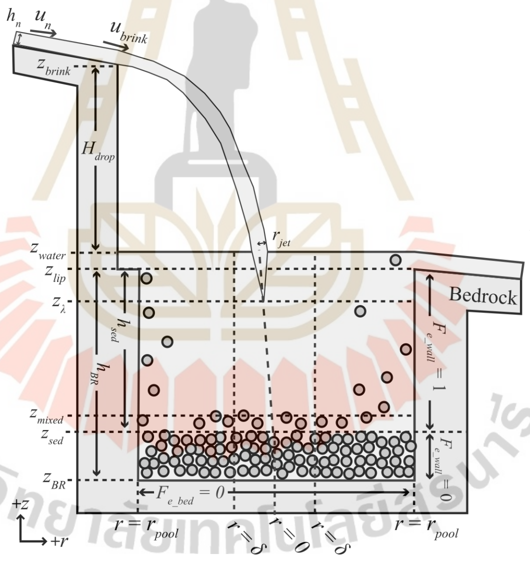

Figure 2.1 Schematic of plunge pool (Scheingross & Lamb, 2017).

Table 2.1 Summarization techniques for accessing the erosion process.

Approach	Technique	Advantage and Limitation	References
Field testing	Erosion rate measurement	• Variation devices for short- and long-term measurements. • The cost for instruments are expensive.	Inkpen and Jackson (2000); Trudgill et al. (1989); Lyles (1983)
	Topography observation	• Highly discontinuous in time are shown along fracture pattern in field. • Persistence of slopes are expressed with a short time scale (typically 0.1-10 Ma).	Krautblatter and Moore (2014)
	Trajectory and distances measurement	• Size effect, properties of rocks, and transportation surface can limit the mobility of rock.	Shrestha (2008); McCarroll and Nesje (1996)
Laboratory testing	Weight loss measurement	• Provide a relative rate. Degradation rate can be calculated with density of rock.	Gapta and Seshagiri (2000); Ergular and Shakoor (2009); Torabi-Kaveh et al. (2021); Torsangtham et al. (2019)
	Surface observation	• Provide a relative value to study the degradation behavior.	Fuenkajorn (2011); Kolay and Kayabali (2006)
	Relative rate measurement from input and output force	• The relative force simulating with field data are concerned • Various of techniques (i.e., Plunge pool, water jet and aerial jet).	George and Sitar (2012); Scheingross and Lamb (2017); Xiang, Latham, and Pain (2022)
Numerical simulations		• Limitation of input and physical parameters of rocks • The effect of scrubbing and colliding of rock need to be concerned	Inkpen (2007)

The mechanisms such as mechanical and chemical erosion are exhibited similarly with weathering. The degradation assessment for erosion process then can be expressed in terms of durability of rocks.

As recommended by the American Society for Testing and Materials Standard, ASTM-D4644 (2016), slake durability index test is one of the techniques for rock durability assessment which indicates the capacity of rock degradation in laboratory conditions.

The mentioning test, originally proposed by Franklin and Chandra (1972) for evaluating the durability and potential to degradation of rock. Their approach utilizes two cycles for wetting and drying of slake tests as the assessment method to observe the degradation capacities by tracking mass loss after each test cycle, the following relationship defines the durability at test cycle i:

$$Id_{\mathrm{i}} = (m_{\mathrm{i}}/m_0)\times 100 \tag{2.1}$$

where Id_{i} is the durability index at test cycle i (%), m_{i} is the mass of a retained samples after test cycle i (g), m_0 is the mass of initial samples (g), and i represent the number of test cycles.

Ergular and Shakoor (2009) analyze statistical relationships between the degradation rate of clay-bearing rocks and grain distribution sizes with the increasing of durability test cycles. Grain size distribution curves are projected to correlate with the concept of disintegration (degradation) ratio, D_R as follows:

$$D_{\mathrm{R}} = A_{\mathrm{C}}/A_{\mathrm{T}} \tag{2.2}$$

where A_{C} is the ratio of area under particle size distribution curves (m^2) and A_{T} is the total area encompassing all particle size distribution curves (m^2).

Zhu and Deng (2019) propose a classification for red beds, clay-bearing rocks from central Yunnan, China. Their classification scheme utilizes both particle size distribution and durability index. The durability index is expressed as:

$$Id_i = (m_i/m_{i-1}) \times 100 \tag{2.3}$$

where m_{i-1} is the mass of oven-dry sample before cycle i. The equation defines relative index based on Franklin and Chandra (1972) but emphasize its effectiveness reflecting the disintegrating capacity on each test cycle.

2.3 Erosional factors

To understand factors governing degradation processes, the approach to assess these alignment factors are reviewed in Section 2.2. In erosional term, not only the externals that are concerned but for internal factors, many researchers try to reach the physical properties of rocks to explain its behaviors. The specific factors controlling such process are alternatively expressed by various researches to reflect the environment matching with their concertation. The relative importance of these factors are varied between field scale and laboratory setting. For laboratory, the specific conditions are controllable to identify the dominant of internal factors, compared to the complex conditions in the environments.

2.3.1. Fluvial factors

Within the context of fluvial systems, Luc, Lomine, Poullain, Sail, and Marot (2015) and Flores, Cuhaciyan, and Wohl (2006) identify dominant factors influencing erosion process include external dynamic energy, scale-dependent relationships, and hydroclimatic controls. Their findings are summarized as follows:

1) External energy

The dynamic energy from water flow, i.e., stream power, influenced by factors such as bedforms and fluid volume in the system. Particle or fragment that reaches high magnitude of energy from a flume bed might exhibit different degradation from those low energy in flat areas.

2) Scale-dependent

Sizes of the streamline are varied depending on patterns of the system. The factor is influenced the reaching distance of particle (fragment) displacing from the initial point. The streamline scale governing particle transport in varies magnitudes.

3) Hydraulic and hydroclimatic parameters

The climatic factors are related to fluid flow through rock matrix, i.e., corrosion, include with the hydraulic shear stress, cohesion between grains, pore fluid pressure, hydraulic gradient and related factors, e.g., rainfall, evaporation, and runoff dynamics within a watershed.

2.3.2. Aeolian factors

Zobeck et al. (2003) analyze the complex of external features governing wind erosion in aeolian environments. The factors involve with the climatic conditions, particle characteristics, and bedform features. Their findings emphasize the importance to consider these factors when assessing wind erosion at the field scale. To clarify this concept, Shrestha (2008) represents a functional relationships to express degradation rates (D) as:

$$D = f(I,K,C,L,V) \tag{2.4}$$

1) Fragment erodibility, I

Erodibility factor represents the susceptibility to erosion, involves with grain sizes, texture, mineral composition and topography feature.

2) Surface roughness, K

Roughness factor accounts for surface irregularities. This factor reducing the erosion by disrupting the impact of wind flow. A rougher surface generally leads to a lower process, representing as a protection against wind erosion. While fragments with higher erodibility tend to lose their surface roughness faster.

3) Climatic erosivity, C

This factor is significant impacted the climatic processes from windspeeds and surface moisture. The calculation for the C factor is represented as $C = 386 \cdot u^3 / (PE^2)$, where u denotes average wind velocity and PE signifies the precipitation index.

4) Unsheltered distance, L

Unsheltered distance represents the distance across a field where erosive winds can freely transport, which directly influenced amount of particles carried by wind power.

5) Vegetation cover, V

The equivalent vegetation cover are accounted for the protective against wind erosion. This factor is determined by comparing the existing vegetation to a reference condition called “Small Grain Equivalent, SGe”. The effectiveness of vegetation for reducing erosion depends on its characteristics.

2.3.3. Laboratory factors

In additional to above considerations, Moses et al. (2014) express that the factors impacting erosion correspond to surface roughness and texture, depth and extent of weathering in matrix, mineral alteration, and rate of material loss from the surface. These results have been confirmed with Gapta and Seshagiri (2000), Lashkaripour and Boomeri (2002), Ergular and Shakoor (2009), Torabi-Kaveh, Mehrnahad, Morshedi, & Jamshidi (2021), and Jamshidi (2023) studies. The degradation rates are varied for different rock types, according to their physical, chemical, and mechanical properties. These factors are summarized as follows:

1) Surface roughness

The erodibility of outer surface, while rocks moving through the systems, e.g., wind and water are increased chance of rock surfaces to interact with environment conditions. The difference of degradation creates surface roughness on a specific rock types.

From findings of McCarroll and Nesje (1996), the variation of degradation rates are influenced from mineral composition and leading to a rough surfaces. The scale of roughness are varied with sizes of mineral grain in the matrix of rock. From their study, three boulders with varying of mineral grain sizes (e.g., 4 cm , 2 cm, and 1 cm) are measured near the cliff and in the splash zone. The results show a significantly altered surface to roughness with a maximum scale of grain sizes, where the transport of boulder fragment (large grain sizes within the matrix) from the cliff to splash zone, tend to have a coarser surface within the process. In Figure 2.2, the fragments are smoothed by marine erosion (below high water). The roughness surface value are maximized mostly near the cliff as shown within a drastically profiles. This agrees with the results obtained by Inkpen (2007), who explained that the impact of erosion on rock surface are depended on the relationship between erosion rates and the height of slope. His results show that the different points of height tend to give more durable to fragments, comparing to a higher degrade of rock surface under flat area. The transport duration of fragment is insignificantly effected the degradation rate. Figure 2.3 shows the simulation of a fragment transport in a different of slope height.

Fuenkajorn (2011) simulates the degradation process of weak rocks including volcanic, metamorphic, and sedimentary rocks with repeated test cycles on the durability test. The results reveal two different patterns based on rock fragment textures (Figure 2.4). Rocks with uniform texture throughout (inner matrix to outer surface) exhibited a relative decrease in durability with test cycles. The uniform texture is suggested on a consistency level of weathering and hardness across the fragment, where a lower durability fragment is degraded faster. Rocks with non-uniform texture tend to have a weaker surface than the inner matrix and results dramatically increased in degradation rate. The transition of rock matrix durability is varied, depending on rock type and weathering degree.

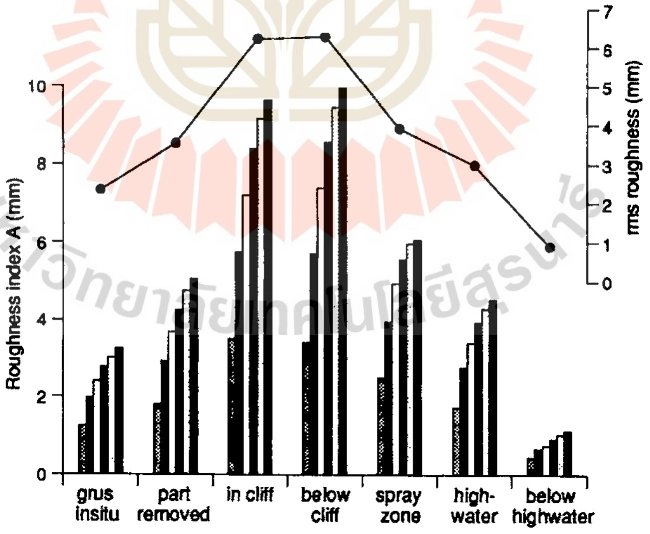

Figure 2.2 Surface roughness profiles in variation systems, the bars represent intervals of 5, 10, 15, 20, 25 and 30 mm, from left to right (McCarroll & Nesje, 1996).

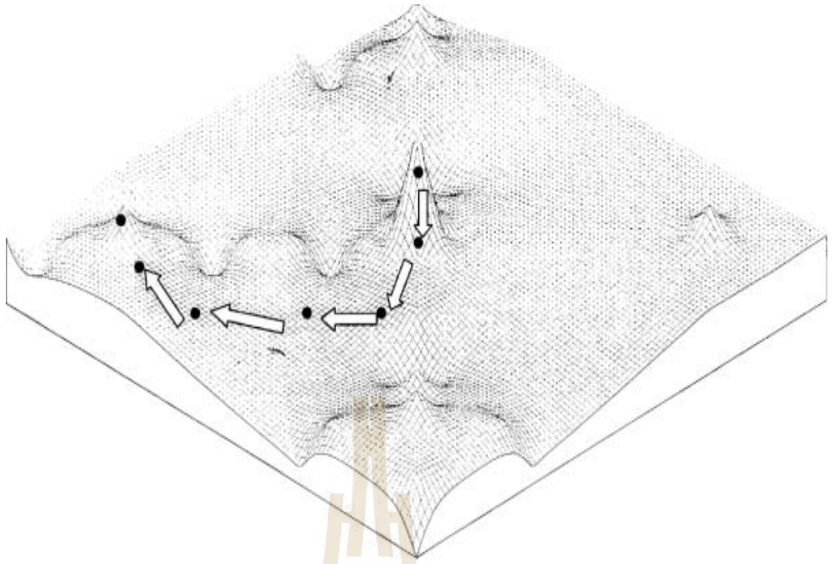

Figure 2.3 Simulation of fragment transport in different points of slope height (Inkpen, 2007).

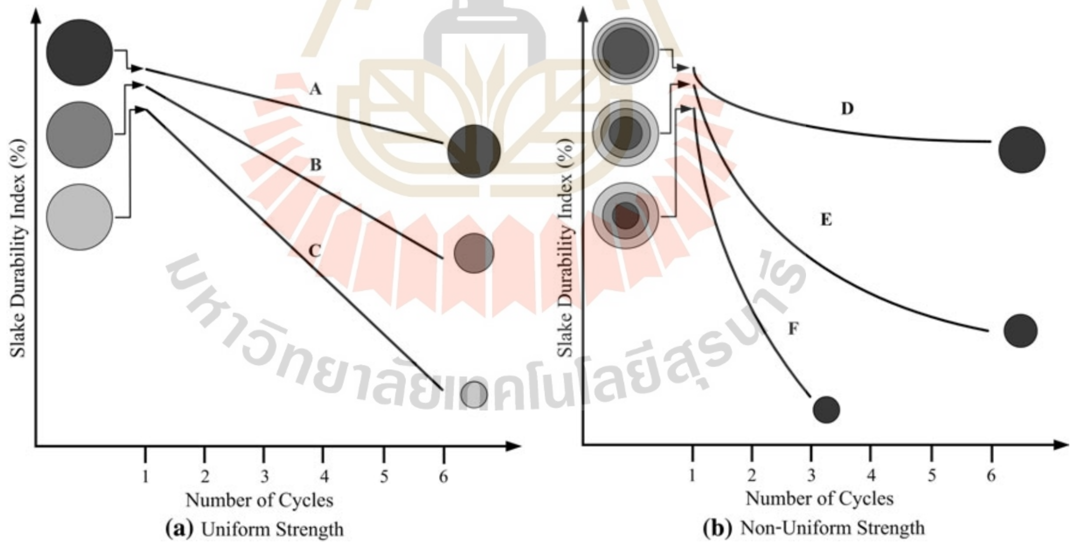

Figure 2.4 Rock degradation concept. Samples A, B and C (a) represent uniform texture. Samples D, E and F (b) represent weathered zone outside and fresher matrix inside (Fuenkajorn, 2011).

2) Mineral alteration

Gokceoglu, Ulusay and Sonmez (2000) correlate relationships of mineral characteristics in weak rocks. They mentioned that clays content, especially smectite, controls the variation of durability. Higher percentage of clays in claystone and ignimbrites causes a significant low durability in the second through fourth cycles from 0 to 70%, where values of durability agree to high carbonate content (Figure 2.5). They also introduce the estimation of quantitative minerals for particles passing from the drum after each slake durability test cycle. The removing rate of these minerals depend on the number of cycles. The cumulative quantities of each mineral (Q_m) is determined as:

$$Q_m = \sum_{i=1}^{i}\{[(Id_i - Id_{(i+1)})(Y_{X_i} / 100)] / Y_{X_0}\} \tag{2.5}$$

where Id_i is the durability index at test cycle i (%), Y_{X_i} is the percentage of each mineral from passing material at test cycle i (%), determined by X-ray diffraction (XRD) analysis, Y_{X_0} is the number of minerals and i is the number of cycles.

They also analyze passing materials with grain size distribution using wet sieve and hydrometer techniques. Their results reveal a significant decrease in fragment sizes correspond to passing materials with increasing test cycles (Figure 2.6). They define that the dominant particle size falls within the silt range, according to the mechanisms of scrubbing and crushing experienced during the tests.

Hawkins and McConnell (1992) investigate physical properties of British Isles argillaceous rocks and find that sandstone is mostly susceptible to water due to clay expansive forces and ferruginous cementing within their matrix. They also determine the quartz-clay framework through the effects of clay content, cementation, and mineral compositions on the durability of sandstones. The results indicated that clay contents contribute to a highly degraded when encounter with water. Ferruginous and calcareous cementations are generally more susceptible than those with siliceous cement under submerging stage. However, they noted that chlorite might play a critical role in strength loss than swelling clay minerals, due to its complicated structure.

The result obtained from Hawkins and McConnell aligns with those of Lin, Jeng, Tsai, and Huang (2005), who study sandstones with significant clay contents. They state that chlorite might be the primary factor influencing the susceptibility of sandstones to degradation during submersion. They give an explanation that it probably due to the leaching potential, which appears to impact than the swelling behavior of clays. According to Figure 2.7, chlorite is significantly loss after subjecting to water, compared to clays contents.

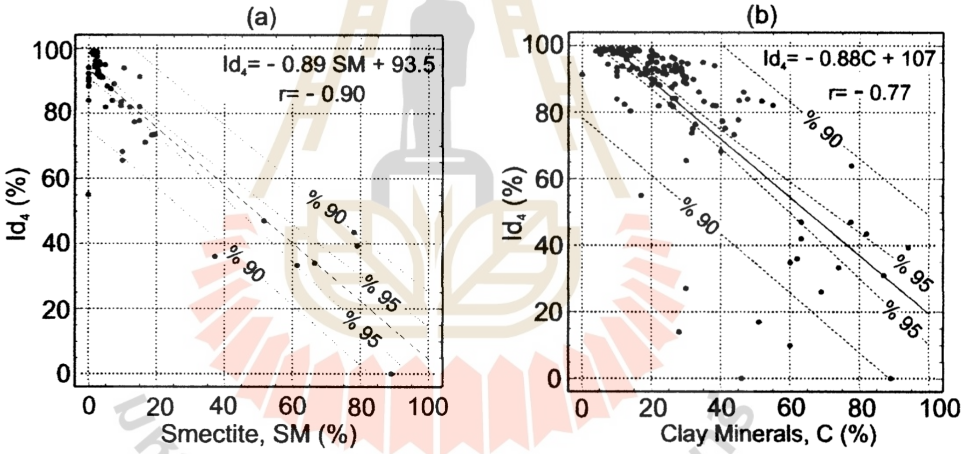

Figure 2.5 Regression of durability with expansive clay (a), and total amount of clay minerals (b) for all rock types (Gokceoglu, Ulusay, & Sonmez, 2000).

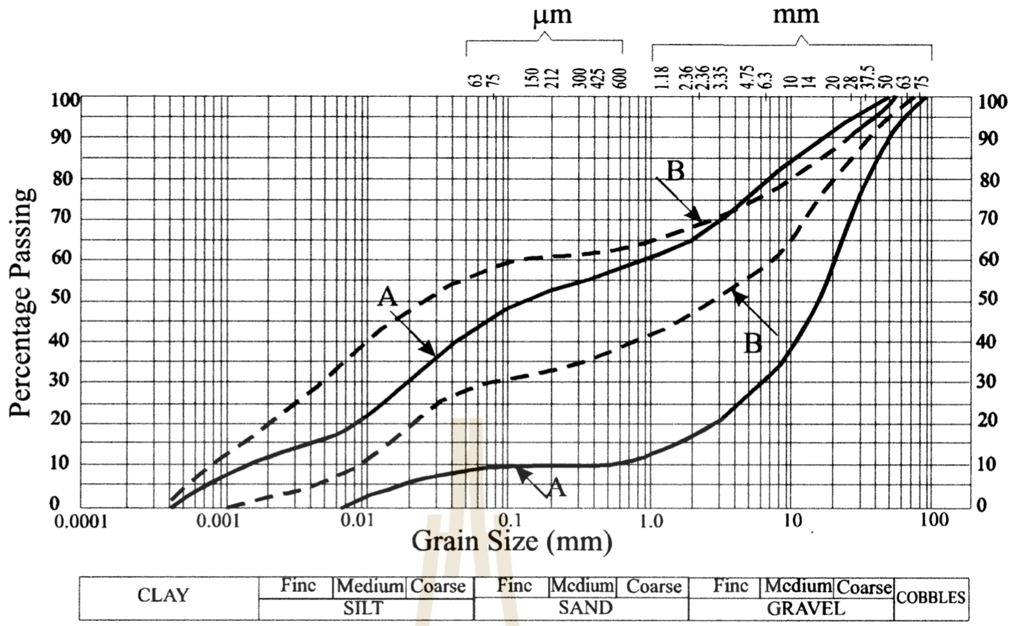

Figure 2.6 Percentage of passing material with a function of grain sizes (Gokceoglu, Ulusay, & Sonmez, 2000).

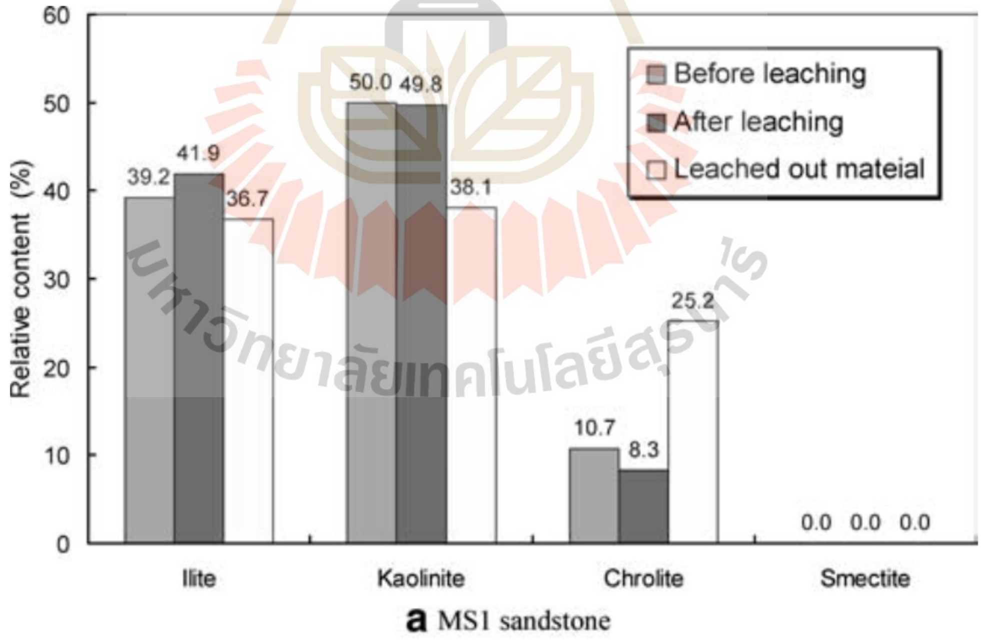

Figure 2.7 Relative clay contents and chlorite in sandstones with variation of stages (Lin et al., 2005).

3) Texture and packing density

Heidari, Momeni, Rafiei, Khodabakhsn, and Torabi-Kavah (2013) state that the effects of rock textures (e.g. fine-grained matrix, grain network, and cementing agent), affect degradation process more than mineral compositions and conclude that rock textures are more noticeable in a relationship for predicted engineering characteristics.

To reveals a significant connection between packing density, grain contact, and porosity, Dobereiner and Freitas (1986) define that grains of sandstones with lower degrees of tangential grain contacts are exhibited floting within the matrix of rock fragment. As packing density increases, the percentage of contacting grains are raised between 25% to 30% causing the strengthen in cementation and internal components inside the matrix. This agrees with Lin et al. (2005), their result shows non-effective of packing density in sandstones with the tangential grain contacts above 60%.

Koncakul and Santi (1999) express a relationship between packing density, porosity, and permeability. They state that the decrease of porosity and permeability are due to packing density that limit the water pass through the matrix and maximizing its durability. The results tend to agree with Corominas, Martinez-Bofill, and Soler (2014) and Sousa, Surarez del Rio, and Calleja (2005), who study the influence of physical properties and microfractures. They conclude that porosity is one of the primary factors that controls the intensity of physical and chemical alterations within rock.

Additional to these factors, the textural feature of rock fragments including their shape and size also affect the erodibility of rock, as evidenced from the results obtained by Gong, Zhu, and Shao (2018), Lamb, Finnegan, Scheingross, and Sklar (2015), and Li, Fu, Hu, and Liu (2022). These studies indicate that the differences of fragment shapes tend to give the alternative results for durability assessment of erosion.

From the study of Kolay and Kayabali (2006), they use the concept of factual dimension to calculate the effect of shapes use in the durability test and conclude that spherical shape exposes less surface area, compared to cubic and triagonal prism shapes. Their results also show that rougher surface further develops a higher angularity. As fragment become less in spherical, the higher of surface area leading change for rock fragment to expose through water and accelerated the degradation process. The relationships between variation shapes are expressed below:

$V_{\text{sphere}} = V_{\text{cube}} = V_{\text{tr. prism}}$

$4.19r^2 = b^3 = 0.43a^2$

giving $r^2 = 0.38b^2$, $a^2 = 1.75b^2$

if $A_{\text{sphere}} = 4\pi r^2$, $A_{\text{cube}} = 6b^2$, and $A_{\text{tr. Prism}} = 3.87a^2$

$A_{\text{sphere}} = 4\pi\,(0.38b^2)$, $A_{\text{cube}} = 6b^2$, and $A_{\text{tr. prism}} = 3.87(1.75b^2)$

$A_{\text{sphere}} = 4.83b^2 < A_{\text{cube}} = 6b^2 < A_{\text{tr. prism}} = 6.78b^2$

where a and b is dimentional axis of cubic and triangonal prism shapes, r is radius of sphere shape (mm), A is surface area of fragment (mm^2), and V is volume of fragment (mm^3). Figure 2.8 shows evaluation parameters within the different geometrical shapes.

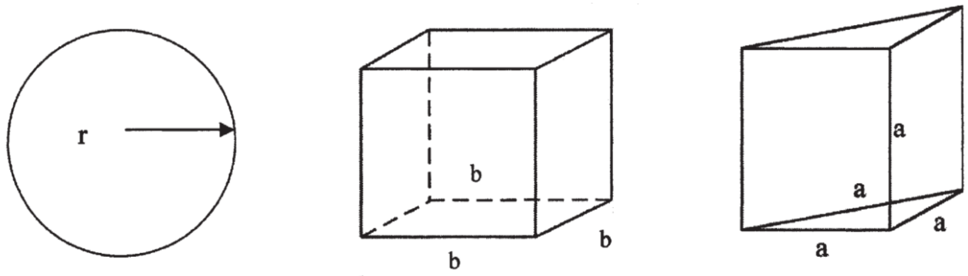

a **Sphere** b **Cube** c **Triangular prism**

Figure 2.8 Geometrical shape parameters of spherical (a), cubic (b) and triangular prism (c), (Kolay & Kayabali, 2006).

4) Pore pressure

The impact of water intrusion on internal structure is weakened the cohesive forces between mineral grains and giving change of water to interact between grains contact, resulting in a reduce of intergranular frictional resistance (Koncagul & Santi, 1999).

According to Lin et al. (2005), who study the micromechanisms of sandstones influenced by the water pressure. They reveal that the presence of water varies the fracture behaviors of sandstones. Sandstones under dry condition tend to propagate cracks within mineral grains (intracrystalline), while saturated sandstones, particularly with low chlorite content, exhibit cracks between grains (intercrystalline). Figure 2.9 shows a variation of fractures occur within sandstones.

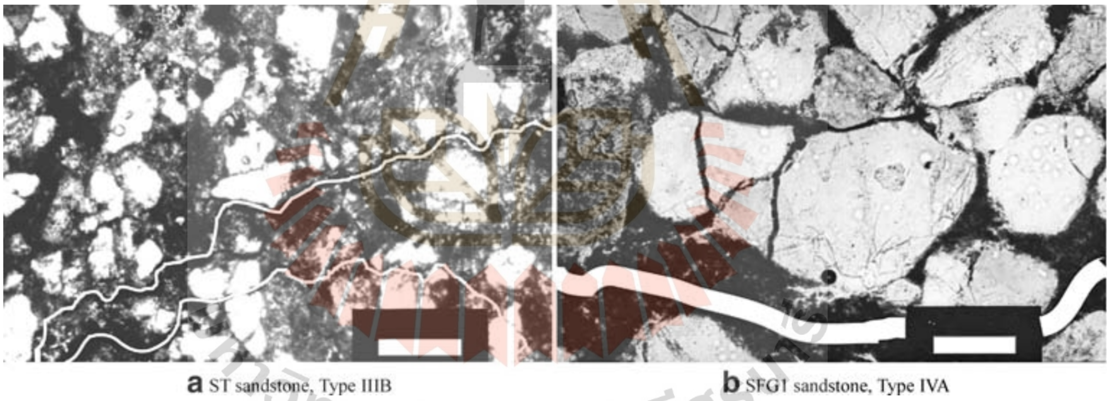

Figure 2.9 Petrographic images of intergranular fracture (a), and intragranular fracture (b) in sandstone (Lin et al., 2005).

5) Internal stresses

The stresses within rock matrix arise from a complex relationship between the factors and correspond to input mechanism in the systems. Current researches have analytically explored the nature of force-induced stresses experienced within rock matrix and upon their surfaces. The inducing forces are considered with many perspectives, including terms of temperature and hydraulic stress.

Thermal expansion induced by the variation change of temperatures to the composing minerals within rocks. Sandstones that contain mostly quartz and feldspar whose thermal expansion coefficients are similar with a high range of heat capacity are more durable (Somerton, 1992). From the study of Li and Liu (2022), Sandstone masses are slightly decreased when temperature is less than 400 °C. They state that high temperature has a significant deteriorating effect, where cracks due to thermal damage show when temperature reaches over 400 °C.

For rocks containing minerals with different thermal properties, such as igneous rocks, the effect of temperature becomes significant. McKay, Molaro, and Marinova (2009) study the degradation behavior influencing by temperature changing on surface of igneous rocks, specified on dry (wind) areas. The thermocouples are used as a site equipment and measure with a constant time intervals (dT/dt). The results obtained from their study shows the similarity distribution of dT/dt values in all conditions. They indicate that thermal stresses from variation of temperatures are significantly cause microcracks and fractures within rock matrix. They also state that the thermal stress might be a significant contributor to the physical spalling and flaking on rock surface.

Tugrul and Zarif (1998), Gokceoglu et al. (2000) and Torabi-Kaveh et al. (2021) give the explanation on the hydraulic stress. Sandstones with clay minerals are directly reduced their durability due to the release of residual stresses within the rock matrix. This release of stress destabilizes the internal structure and accelerates its degradation during submersion.

6) Duration and replete cycles

The duration of testing is significance for assessing durability. Lin et al. (2005) explain the assessments with extended periods, revealing that the degradation rates are increased with prolonged submersion, which directly cause more interaction time between water and internal structure of rocks. They also state that the densities are decreased around 0.5 g/CC after a period of submersion. As the porosity increases, the mineral contents within the matrix appear to become less cohesive and easily to reach out with water (Figure 2.10). This finding agrees with the results of Zhou, Cai, Ma, Chen, Wang, and Tan (2018), they observe water ingression into the matrix of sandstones, within 24 hours the percentage of water is linearly increased up to 3% (Figure 2.11). Their results show that after repeating of cycles, the durability and density tend to decrease with an increasing of porosity, where it corresponds with the submerging time (Figure 2.12).

Gokceoglu et al. (2000) investigate the influence of test cycles on durability for various rock types from Turkey. The statistical analyses from their results are utilized as the influence of cycles on the degradation rate. The results show that the coefficient between these relationships is relatively increased with test cycles, causing the intergranular bond to become weakening and developed the microcracks within rock matrix.

This agree with the results obtained by Fereidooni and Khajevand (2017) and Torsangtham, Khamrat, Thongprapha, and Fuenkajorn (2019), who investigate rock durability through 100 cycles of a slake durability tests under wet, dry, and acidic conditions on carbonates, granites, sandstones, and basalts. The results show that in long-term, granite durability deteriorates under exposure through water and acidic conditions, due to their structures such as pore matrix and ferrous oxide cementation, which leading to microcracks. The study also reveals that sandstones degrade highest under wet conditions due to expansive clays in their matrix.

Walsri, Sriapai, Phueakphum, and Fuenkajorn (2012) simulate sandstones degradation using a large-scale slake durability test device and perform 100 cycles under dry and wet conditions. Test results show the sensitivity of sandstones are severed as submerged in a prolong cycles. The degradation rate after submerging to water is increased than under dry condition.

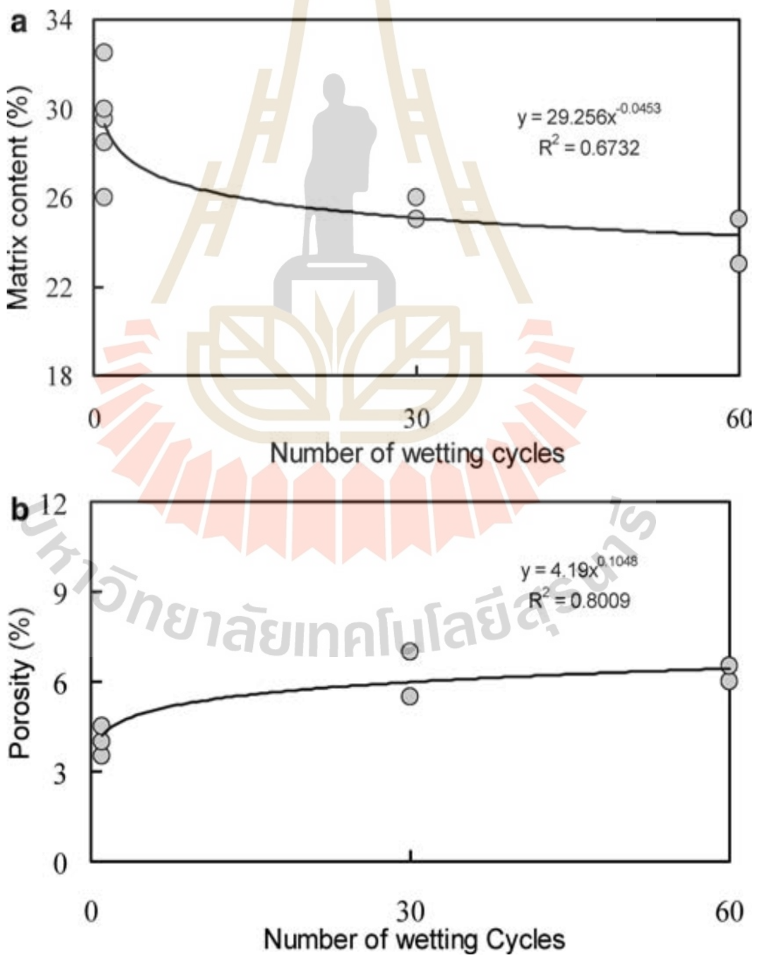

Figure 2.10 Influence of cycles to matrix content and porosity of sandstones (Lin et al., 2005).

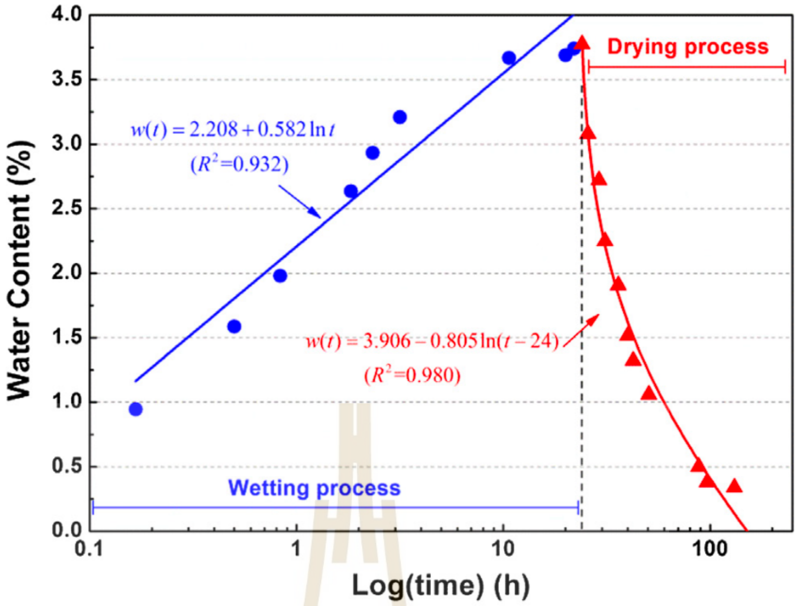

Figure 2.11 Water content in a function of time duration (Zhou et al., 2018).

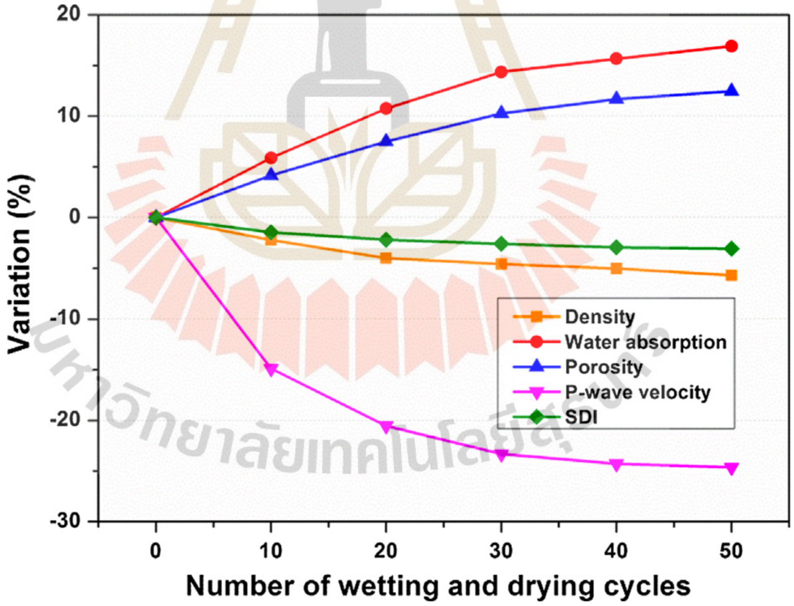

Figure 2.12 Percentage of variation properties with a number of wetting and drying cycles (Zhou et al., 2018).

2.4 Erosive energy

Mathematical evaluation of energy requisites for rock degradation is developed with multi-perspectives. The current approaches to resolve energies are incorporated in a wide range of concepts across many disciplines, considered reflective to environment conditions. Recent researches attempt to define the connection between energy and degradation mechanisms with field monitoring data, visual observation, and simulation techniques (detailed in section 2.2). To clarify the perspective, the reviews are focused on the classification of processes, while the origin of forces are addressed in a subsequent section.

2.4.1 Wind process

Aeolian degradation process, or wind erosion is influenced by a complex factors (detailed in 2.3). The sufficient volume of windspeeds can transport the fragment or particle through saltation, creep, or suspension. Lyles (1983) defines the erosive wind energy using extensive field data from aeolian area in North America. She uses the erosive potential from windspeeds profile to estimate the annual erosion rate. The following equation is determined the relationship of energies as:

$$E_p = (EWE)\cdot(E_a) \tag{2.6}$$

where E_p represents estimated erosion over a defined period (mm/yr), EWE is proportionality constant reflecting erosive wind energy at a specific location (J), and E_a is the estimated annal erosion (mm/yr). She state that terrain and temperature need to be concerned, where the temperature below subzero causes particles in solid state.

Shrestha (2008) develops an equation to estimate erosive wind energy (EWE) with an hourly windspeeds data. The equation is expressed as:

$$EWE = 3600 \cdot \rho \cdot (U^3 - U_T^{\,2}) \tag{2.7}$$

where *EWE* is the hourly erosive wind energy (J), ρ is the wind density (g/m), U and U_T are the average hourly windspeeds and average hourly threshold windspeeds (m/s), respectively.

2.4.2 Stream (Water) process

Larimer, Yager, Yanites, and Witsil (2020) investigate the energy transfers by mechanical impacts during particles and observe the saltation behavior on planar and non-planar bed surfaces. They propose the equations defining rates of kinetic impact energy, which involving with the magtitude impact of the energy and rate of impaction. The relative equtions are state as follows:

$$\varepsilon_{kr}^{*} = \frac{q_s\,[\sin(\vartheta - \varphi) \cdot V_{si}]}{2 \cdot R_b\, g\, l_s} \tag{2.8}$$

where R_b is the buoyant density of particle (g/cc), g is gravity, h_s is the hop height (m), v_{si} is the vertical settling velocity (m/s), l_s is the horizontal displacement (m), ϑ is the angle relative to average bed slope (degrees), and φ is the surface angle of bedding (degrees). They state that the proposing equation is maximized the influence of non-dimensional transport. The relative factors include hydrodynamic forces, particle weight, relative fluid motion, particle rotation, and collisions with the bed and other grains. To address this complexity in relationship, the following are expressed in terms of transport trajectory (Wiberg & Smith, 1985):

$$T^{*} = \frac{\rho_w\, g\, R_h\, S}{(\rho_s - \rho_w)\, g\, D_s \cdot \tau_c^{*}} - 1 \quad , \tag{2.9}$$

where τ_c^{*} is the critical stress, ρ_W is water density, ρ_S is particle density, R_h is hydraulic radius, S is channel slope. From Wiberg and Smith, there are three factors related between saltation mechanisms (Figure 2.13):

the hop displacement:

$$l_s^* = \frac{l_s}{D_s} \ , \tag{2.10}$$

the hop height:

$$h_s^* = \frac{h_s}{D_s} \ , \tag{2.11}$$

and vertical-independent velocity:

$$v_{si}^* = \frac{\sin(\vartheta - \varphi) \cdot V_{si}}{\sqrt{(R_b\, g\, D_s)}} \tag{2.12}$$

According to the relationship of aforementioned equations. Wiberg and Smith state that the stress is significantly influenced the energy dynamics. The duration of particle transports directly corresponded with the rate of particle velocities. The displacement of particle hopping decreases the dynamic of kinetic energy to bed load. They note the effect on flow direction, considered on the turbulence flow through the trajectory. The machanism of saltation with high inertia in the matrix seem to diminish the fluctuations. However, for interpretating on the kinetic energy impact, the fluctuation effect still needs to be concerned.

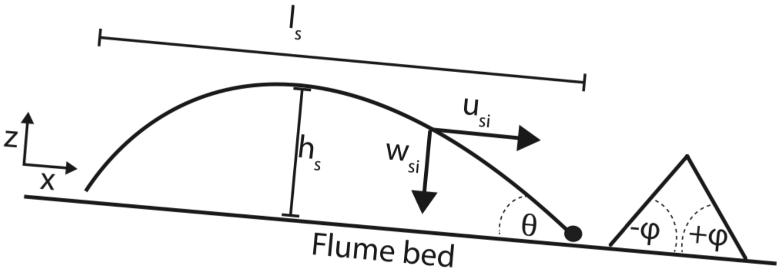

Figure 2.13 Saltation trajectory diagram (Larimer et al., 2020).

Marot, Le, Garnier, Thorel and Audrain (2012) propose a streamline approach to study the process and symplify the equation based on concept of fluid energy on fragment (particle) with diameter between 0.5 µm to 0.125 mm. They state that the relationship emphasizing on mechanical aspect as given parameters, including temperature and internal energy (intrafluid and pressure) in steady-state condition. The total energy dissipated from water flow are determined by integration of the erosion power (P) over the test duration as follows:

$$\frac{dE}{dt} = \frac{d}{dt}\int P = \frac{dW}{dt} = (\rho \cdot g \cdot \Delta z \cdot K) + (K \cdot \Delta P) \qquad (2.13)$$

where E is the total energy (J), W is work in process, ρ is density of fragment (g/cc), g is gravity, Δz is the distance of fragment transfers in the system (mm), K is fluid flow rate, and ΔP represent the power done in time duration. According to their analysis, the total energy varies from 40 to 490 J. They suggest that total energy under 60 J for fragments with diameter less than 0.125 mm (clay size) has no significant erosion that should be measured. They also correlate eroded mass with total energy dissipation (Figure 2.14). The results show that the quantity of eroded mass (g) exhibits a linear correlation with energy dissipation and can be expressed as m_{erode} = 0.0017(E - 60).

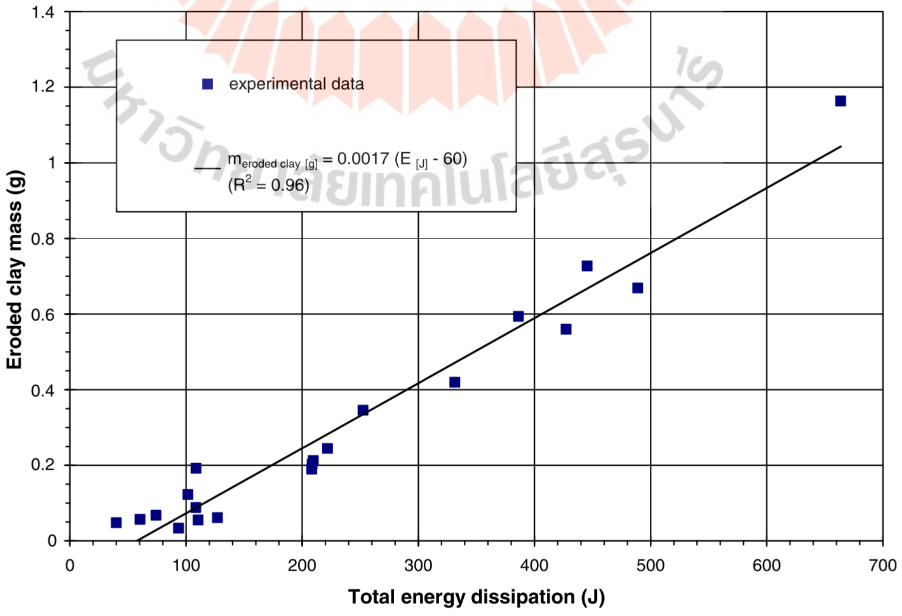

Figure 2.14 Eroded mass in a fuction of total energy dissipation (Marot et al., 2012).

Luc et al. (2015) analyze the internal erosion of rock fragments under water seepage and while fragments transport in the systems. They observe fragment behavior by deviding the processes as internal shear stress and flow power energies. The shear stress can be defined as:

$$\frac{d\varepsilon}{dt} = k_d \cdot (T_s - T_c), \qquad \text{if } T_s > T_c \tag{2.14}$$

where ε is rate of erode mass per unit of erosion surface area, k_d and T_c are parameters characterizing the sensitivity of the soil erosion, and T_s is hydraulic shear stress

Fuenkajorn (2011) proposes an energy absorption concept and correlates the simulation of durability test cycles with field data. The following equation is developed to evaluate heat energy absorbed by rock specimens as:

$$Q = \sum_{i=1}^{n}(m \cdot C_p \cdot \Delta T_i \cdot \Delta t_i) \tag{2.15}$$

where Q is absorbed energy of specimen (kJ), m is mass of specimen (kg), C_p is specific heat capacity (kJ/kg·K), ΔT_i is temperature change in Kelvin degrees, Δt_i is the time interval of energy absorption (hours) and n is the number of hours. The energy absorbed during heat simulation for a common rock is estimated as 4.320 MJ/h (where m = 5 kg, C_p = 0.90 kJ/kg K, ΔT_i = 80 K, and t = 12 h) and the coefficient of heat capacity varies between 0.6 and 1.2 kJ/kg·K. The limitation on variation change of temperature during simulations might induce damage to rock matrix compared to the gradual changes observing in field.

CHAPTER III

ROCK SAMPLES

This chapter describes geological of selective area and sample preparation for Phra Wihan siltstone, Phu Phan conglomeratic sandstone and bedded sandstone.

3.1 Sample collecting and geological area

Samples have been collected from Northeast part of Thailand. Geological strata in this area is mostly comprised with Mesozoic red bed sedimentary rocks. Mainly composed of conglomeratic, sandstone, siltstone, mudstone, and shale. Somes of the strata have interlayers of rock salt and potash, which likely found across south China, Laos, and other countries nearby (Zhou et al., 2019; Song et al., 2017). In Thailand, Two basins are identified to have these strata, known as Khorat and Sakon-Nakhon basins. From recent studies, both basins tend to have good geological correlation with less of hiatus (Charusiri, Imsamut, Zhonghai, Ampaiwan, & Xu, 2006; Racey, 2009). Before Triassic-Jurassic tectonic genesis, some researchers believed that these basins used to coexist as one. After the event, Phu Phan ranges were uplifted and separated both apart (Veeravinantanakul, Kanjanapayont, Sangsompong, Hasebe, & Charusiri, 2018). Khorat basin is known as one of a complete Mesozoic red bedded series. The series of formation, comprise with Nam Phong, Phu Kradung, Phra Wihan, Sao khua, Phu Phan, Khok Kruat, Maha Sarakham and Phu Tok formations. These formations deposited upward, respectively. This study will be focused on sedimentary rocks in Khorat basin, especially at the West edge.

The selected samples are from slope embankment and road cut in Nakhon Ratchasima and Chaiyaphum provinces, coordinate zone 47N locate at 101°68’11” E /

15°56’35” N and 101°52’30” / E 14°40’15” N. The samples included with the upper part Phra Wihan sandstone (PWSS) and conglomeratic sandstone (PPCS) and bedded sandstone (PPSS) from the lower part of Phu Phan formation. Selective areas and northeastern railway lines (State Railway of Thailand [SRT], 2020) are shown in Figure 3.1 with geological formations of the Khorat group (Department of Mineral Resources [DMR], 2018).

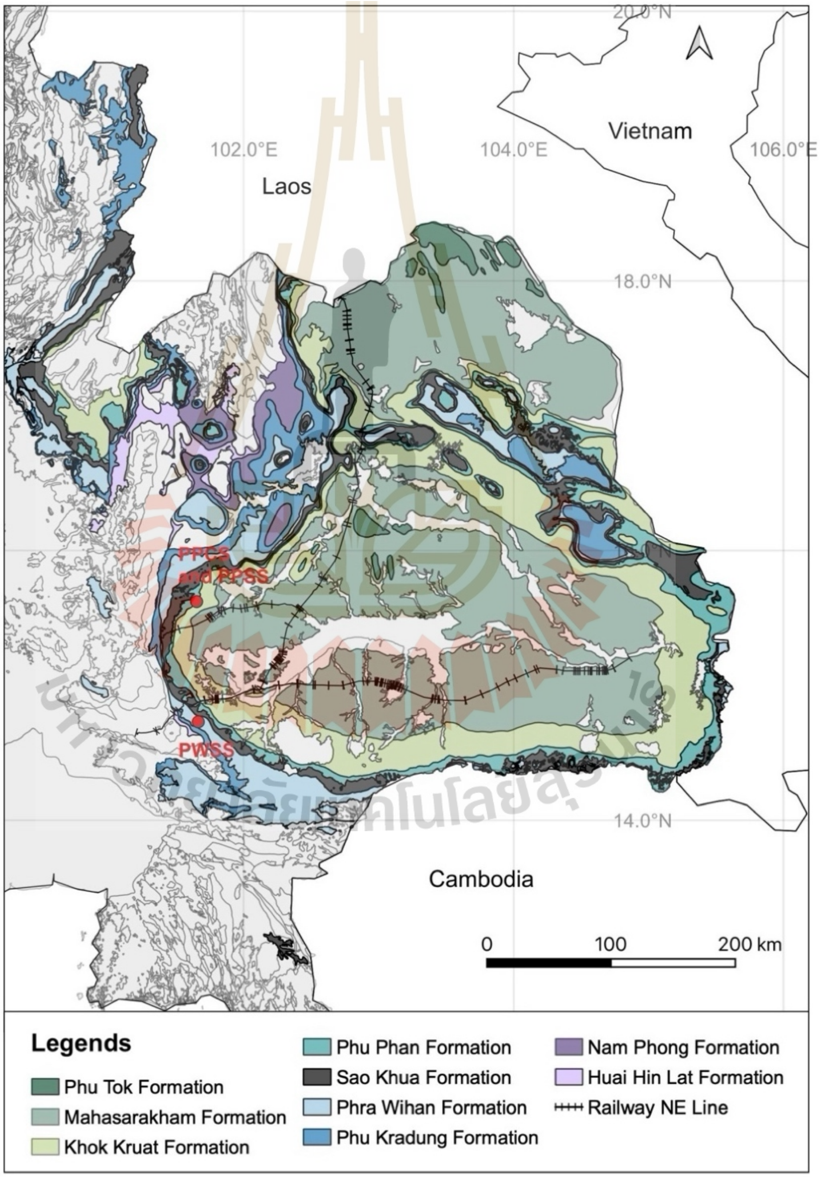

Figure 3.1 Geological map of sample collecting area (modified from DMR, 2018; SRT, 2020).

3.2 Sample preparation

Rock specimens of Phra Wihan sandstone (PWSS), Phu Phan conglomeratic sandstone (PPCS) and Phu Phan bedded sandstone (PPSS) are cut to obtain cubical blocks with dimensions of 27.5×27.5×27.5, 25.0×25.0×25.0, and 29.5×29.5×29.5 mm^3, respectively. Twenty cubical specimens have been prepared for each rock type. The specimens are remained smooth surface with discrepancy of grinding ± 0.5 mm in each axis. Ten specimens are used for dry slake durability index test, and the rest for wet testing. The combined dry weight of ten specimens is about 500±50 g, following ASTM D4644-16 standard. The specimens are prepared with bedding planes parallel to one of the specimen side. Figure 3.2 shows representative of initial specimens in each rock types and Figure 3.3 shows specimens of PPCS using under dry testing. The average density of PWSS is 2.35 g/cc and 2.67 g/cc and 2.53 g/cc for PPCS and PPSS. The density is determined in accordance with ASTM D2763-21 standard test method.

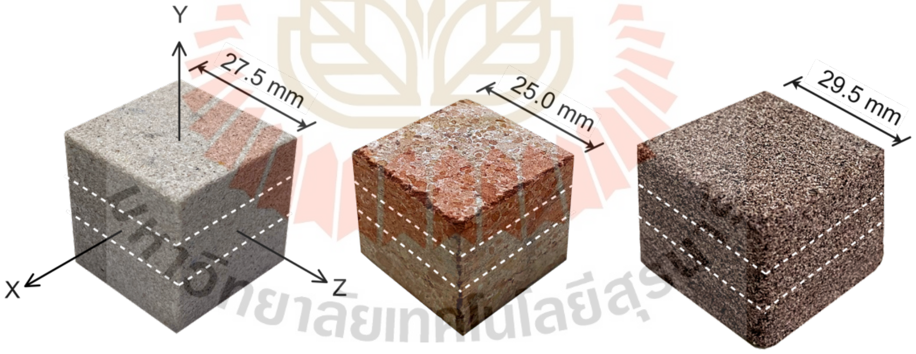

(a) (b) (c)

Figure 3.2 Representative of specimens at initial condition of PWSS (a), PPCS (b), and PPSS (c) with dimensions. Dash lines show alignment of bedding planes.

Figure 3.3 Examples of PPCS specimens prepared for dry testing.

3.3 Mineralogical and petrographic examination

This section includes the result of mineralogical and petrographic analysis at initial condition. The mineral compositions of rocks are obtained from X-ray diffraction (XRD), analyze based on the Rietveld refinement method as specified by ASTM E3294-22 standard. The samples are prepared with sizes less than 0.42 mm. (mesh no. 40). The sizes are prepared such that to provide more prospect of X-ray beam to contact with the surface. The sample is contained in sample holder (Figure 3.4) and tested with Rigaku smart lab X-ray diffractometer by using Cu-Kα tube (1.5418 Å) with 0.5 sec/step. The specified interest two theta are ranging from 5-80 degrees. The results of mineral compositions at initial conditions are shown in Table 3.2.

Petrographic examination provides more accuracy to identify mineral compositions within rocks. The results of both tests will be correlated to classify as if they are grains, matrix or cementing materials. The samples are prepared normal to mirror plate and grinding until the sample thickness is 0.3±0.05 mm. The result shows in Figure 3.5 represented the image of cross polarized light and closed up image of specimens. The images show that PWSS specimen has a grain contacts with siliceous cementing. PPCS specimen shows matrix supported of quartz and some of calcite minerals with lithic fragments and calcrete feature. For PPSS specimen, ferrous oxide appear to be a cementation of quartz, feldspars, and other mineral grains.

Table 3.1 Mineral compositions of samples before testing.

Mineral compositions		Weight percent (%)		
		PWSS	PPCS	PPSS
Quartz		78.58	14.13	60.60
Plagioclase feldspars		1.99	6.81	5.93
K-feldspars		3.00	2.86	0.74
Mica	Biotite (Mg-Fe)	1.89	2.31	0.26
	Muscovite (K)	0.97	0.45	2.21
Clays minerals	illite	0.64	5.36	1.30
	Kaolinite	5.74	2.37	1.70
	Montmorillonite	0.58	0.61	0.31
Chlorite		4.32	2.01	9.22
Calcite		0.23	58.28	11.32
Dolomite		0.00	0.77	0.80
Gypsum		0.81	1.97	2.54
Siderite		0.00	0.29	0.36
Goethite		0.00	0.00	0.68
Hematite		0.22	1.86	1.54

(a) (b) (c)

Figure 3.4 Sample preperation for XRD analysis of PWSS (a), PPCS (b) and PPSS (c).

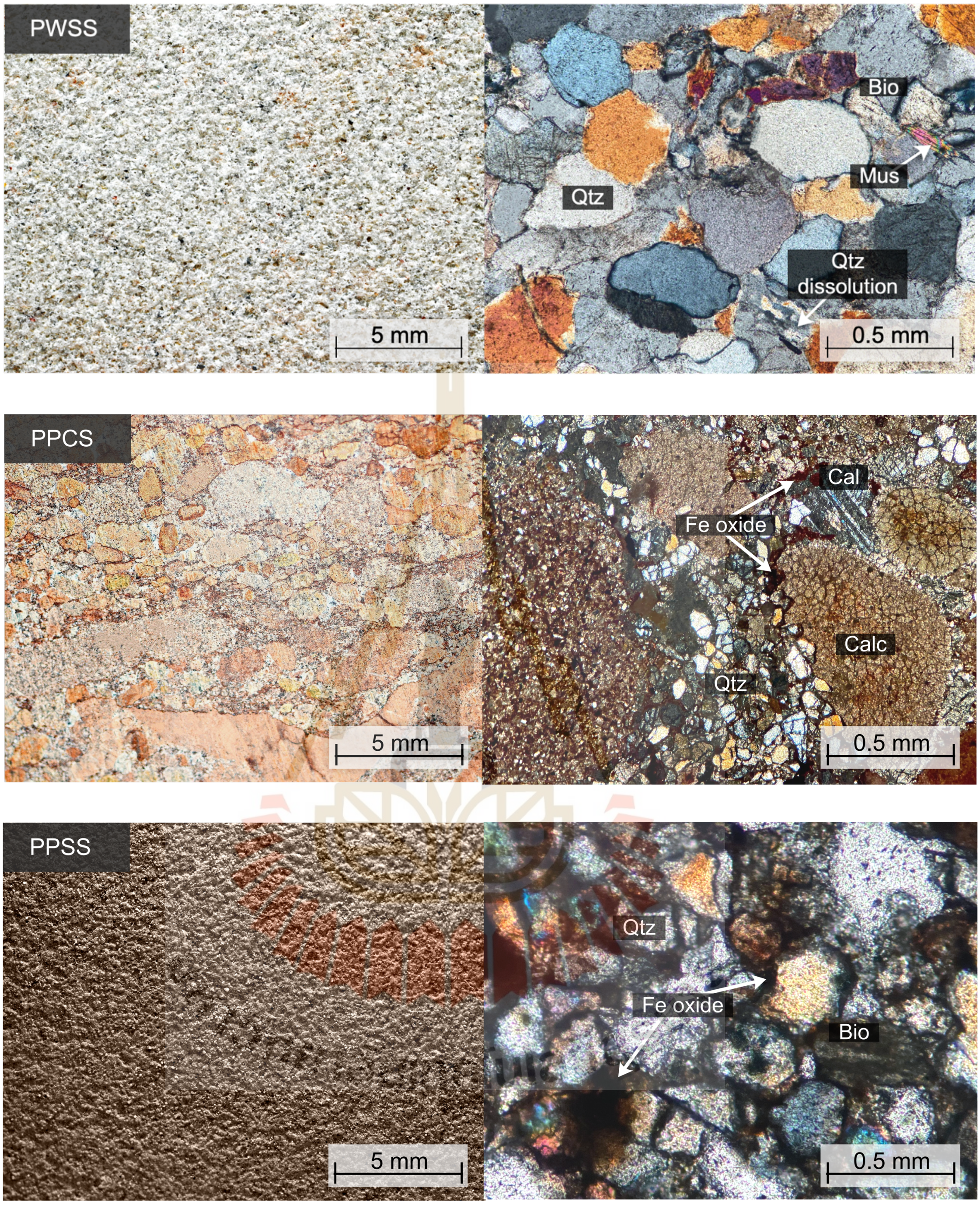

Figure 3.5 Closed-up images of specimens (right) and petrographic images under cross polarized light (left) of PWSS, PPCS and PPSS. Quartz (Qtz), Calcite (Cal), Calcrete (Calc), Muscovite (Mus) and Biotite (Bio).

CHAPTER IV

LABORATORY TEST AND PHYSICAL MEASUREMENT

This chapter describes methodology, and calculations involving the laboratory testing and physical measurements. Laboratory tests emphasize determining the durability index and density. The fragment sizes and shape are measured to identify the change of rock fragments. The equations for evaluating the weight percent of passing materials are proposed.

4.1 Test scheme

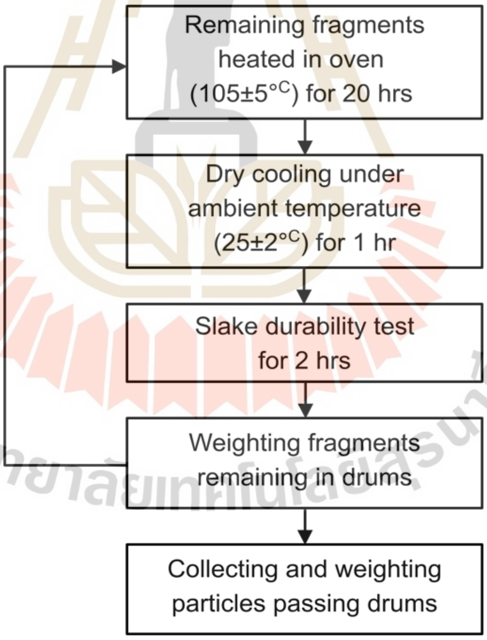

Figure 4.1 Diagram representing one test cycle

According to the diagram of schematic process in Figure 4.1. Two sets of fragments for all rock types are subjected to the slake durability index test: one under dry condition, the other under wet condition. The test duration is about 2 hours (included the process of drums installation) Before testing in the next cycle, fragments in both conditions are left air-cooled at ambient temperature (25±2°C) for 1 hour, after heated in the oven under temperature of 105±5°C for 20 hours, the weight is measured. After each test cycle, particles that pass through the opening from every test cycles and the remaining fragments in the drum from test cycle 80 are collected for further mineral analysis.

4.2 Slake Durability Index test

The durability test and calculation follow the standard test specifications in accordance with the American Society for Testing and Materials, ASTM D4644-16 (ASTM, 2016). Figure 4.2 shows the test apparatus used in this study. A detailed schematic diagram of the apparatus is presented in Figure 4.3. The device comprises with 2 rotating drums. Each with a diameter of 140 mm and length of 100 mm, connecting to the controller with an axle. The drums are wraped with 2 mm mesh wires with a constant rotational speed of 20 rpm. Figure 4.4 illustrates the cross section and side view of the drums.

The test is modified from the standard by using a different shape of fragments from irregular lump to cubic. Every cycles are tested beyond the standard by increasing the drum rotations from 200 to 2,000 revolutions and tested for 80 cycles instead of 2 cycles. This is to accelerate the erosion process of the fragment specimens.

The durability index for each test cycle are determined as $Id_i = (m_i/m_0)\times 100$, where m_i is the total mass of fragments retained after test cycle i (g), m_0 is the total mass of fragments before test cycle i (g), and i is the number of test cycle.

To evaluate the relative values for passing materials in each test cycle. The total mass loss between each cycle is defined as particles that pass through the drum opening. The passing materials are calculated as:

$$P_{\mathrm{i}} = m_{\mathrm{i}} - m_{\mathrm{i-1}} \tag{4.1}$$

where P_{i} represents mass of passing materials from test cycle i (g).

To determine accumulative percentage of passing materials, P_{A}. The following calculation can be applied:

$$P_{\mathrm{A}} = \sum_{\mathrm{i=1}}^{80} P_{\mathrm{i}} \tag{4.2}$$

The aforementioned relationship serves as a standardized to compare rocks with variation of initial mass. To correlate with the durability index, the relative percentage of cumulative passing materials are represented by the following equation:

$$\mathrm{P_A} = (\mathrm{P_i} / \textstyle\sum_{\mathrm{i=1}}^{80} P_{\mathrm{i}}) \times 100 \tag{4.3}$$

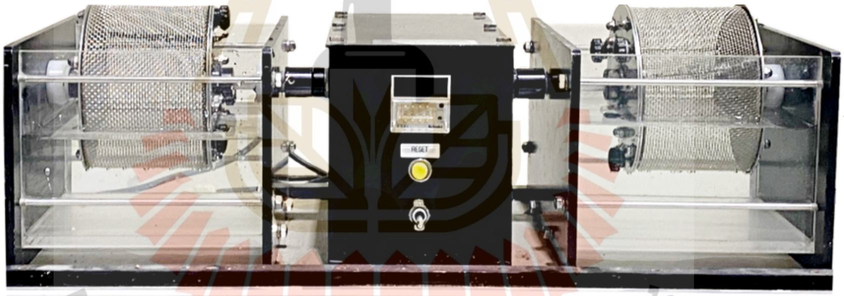

Figure 4.2 Slake durability index test apparatus.

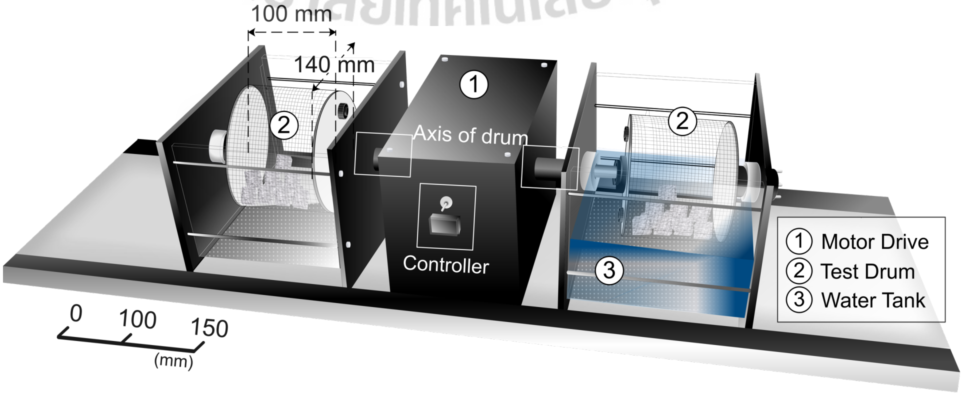

Figure 4.3 3D schematic diagram for durability test.

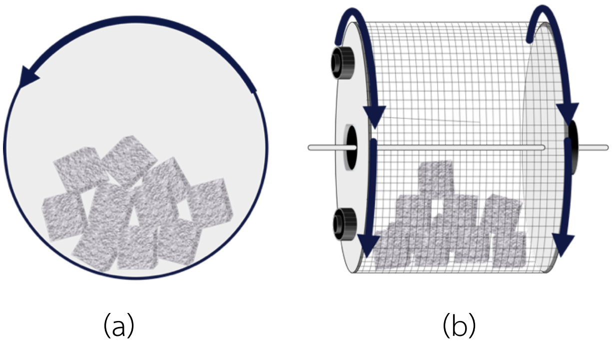
(a) (b)

Figure 4.4 Cross section and side view of drum with rotational direction.

4.3 Density

The calculation of density for fragments under wet condition are from volume displacement technique, as suggested by ASTM D7263-21 standard test method. To consider the potential of water ingressing into fragment matrix under dry condition that might impact the erosion process. The density for fragment under dry condition can be calculated in term of mass subtracting by volumatic change of fragments. The equation is

4.4 Physical measurement

Shape determination follows the established method from Hryciw et al. (2016). The parameters utilized in this study include:

the roundness:

$$R = (\textstyle\sum_{i=1}^{80} r_i /n) /r_{ins} \qquad (4.4)$$

where r_i is radius of circles filled to corners of each fragment (mm), r_{ins} is largest radius of circle fitted to the entire fragment (mm), and n is the number of corners (Figure 4.5a), and the sphericity:

$$S = d_2/d_1 \qquad (4.5)$$

where d_1 and d_2 represent the widest and narrowest diameters of each fragment, as shown in Figure 4.5b. The illustration classifications in Figure 4.6 are modified from

Hryciw et al. (2016) used for further tracking of shapes discussed in the next chapter. The roundness and sphericity classifications are shown in Table 4.1 through 4.2.

Fragment size assessment is obtained from three mutually perpendicular axes of the fragment, i.e. longest, intermediate, and shortest across each fragment in both conditions. The average fragment size is determined by calculating mean of these values. The measuring technique is the same as presented for sphericity (See Figure 4.5b).

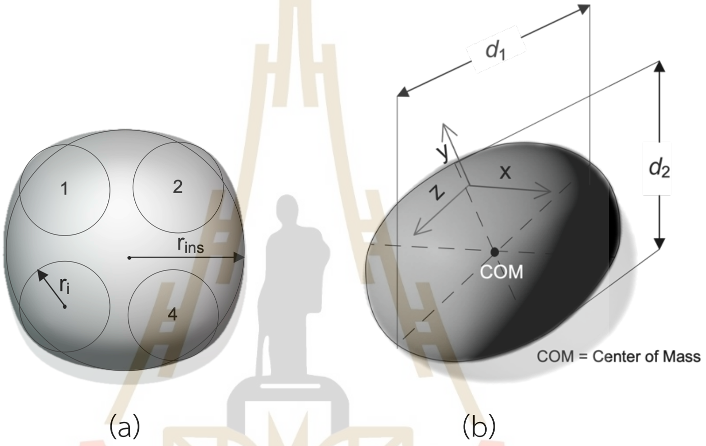

Figure 4.5 Dimensional parameters for roundness (a) and sphericity (b), (modified from Hryciw et al., 2016).

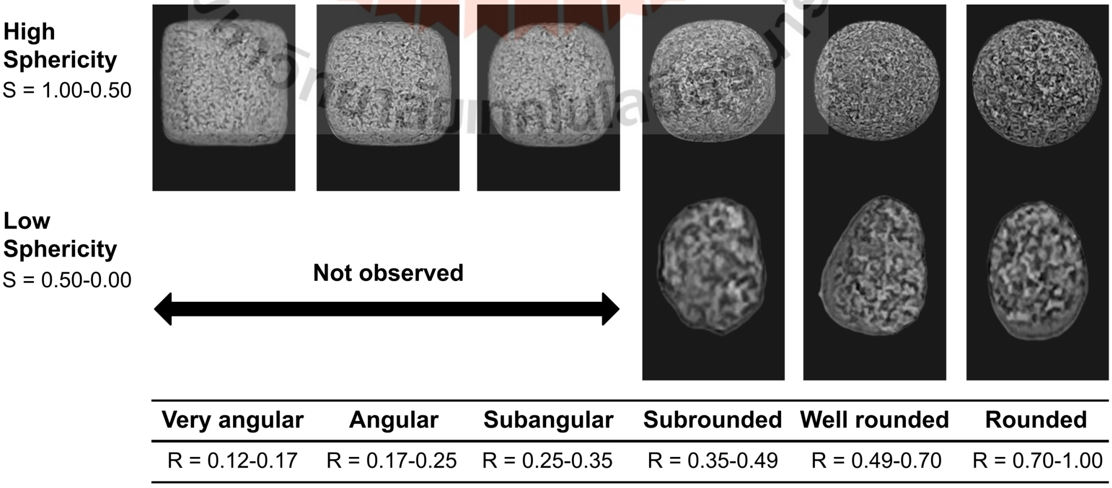

Figure 4.6 Classification for surface roundness and sphericity (modified from Hryciw et al., 2016).

Table 4.1 Roundness classifications (Hryciw et al., 2016).

Classification	Value
Very angular	0.12-0.17
Angular	0.17-0.25
Subangular	0.25-0.35
Subrounded	0.35-0.49
Well rounded	0.49-0.70
Rounded	0.70-1.00

Table 4.2 Sphericity classifications (Hryciw et al., 2016).

Classification	Value
High	1.00-0.50
Low	0.50-0.00

CHAPTER V

TEST RESULTS

This chapter represents the results of three rock specimens during and after test through 80 cycles of slake durability index test. The obtained data includes (1) shape and size of specimens, (2) passing materials, (3) mineral compositions, and (4) fragment density measured for an interval of 20 cycles.

5.1 Specimen shape and size

The physical changes of PWSS, PPCS, and PPSS fragments under dry and wet tests are illustrated in Figure 5.1. The images show the representative of the specimens prepared before testing and those remaining in the drum after subjecting to the durability tests for 20, 40, 60 and 80 cycles. Under both conditions, all fragments become rounder and smaller as the test cycles progress. PPCS and PPSS specimens under dry tests are deteriorated less under than wet condition. However, it seem that PWSS specimens might be smaller in dry conditions than those subjected to water. Under wet condition, PPSS specimens significantly smaller than PPCS and PWSS specimens. By the test cycle 40, PPSS specimens are flattened, where their larger dimensions are parallel to the bedding planes. After 80 test cycles, fragments seem to be degraded normal to bedding plane and show more rounded pattern. PPCS specimens under wet condition show a rough surface on fragments within the first 20 cycles of durability testing. These fragments become smoother after 40 test cycles. Three dimensional models for a representative fragments under wet testing are available via QRcode. For each fragment visualization, figures are shown in Appendix A.

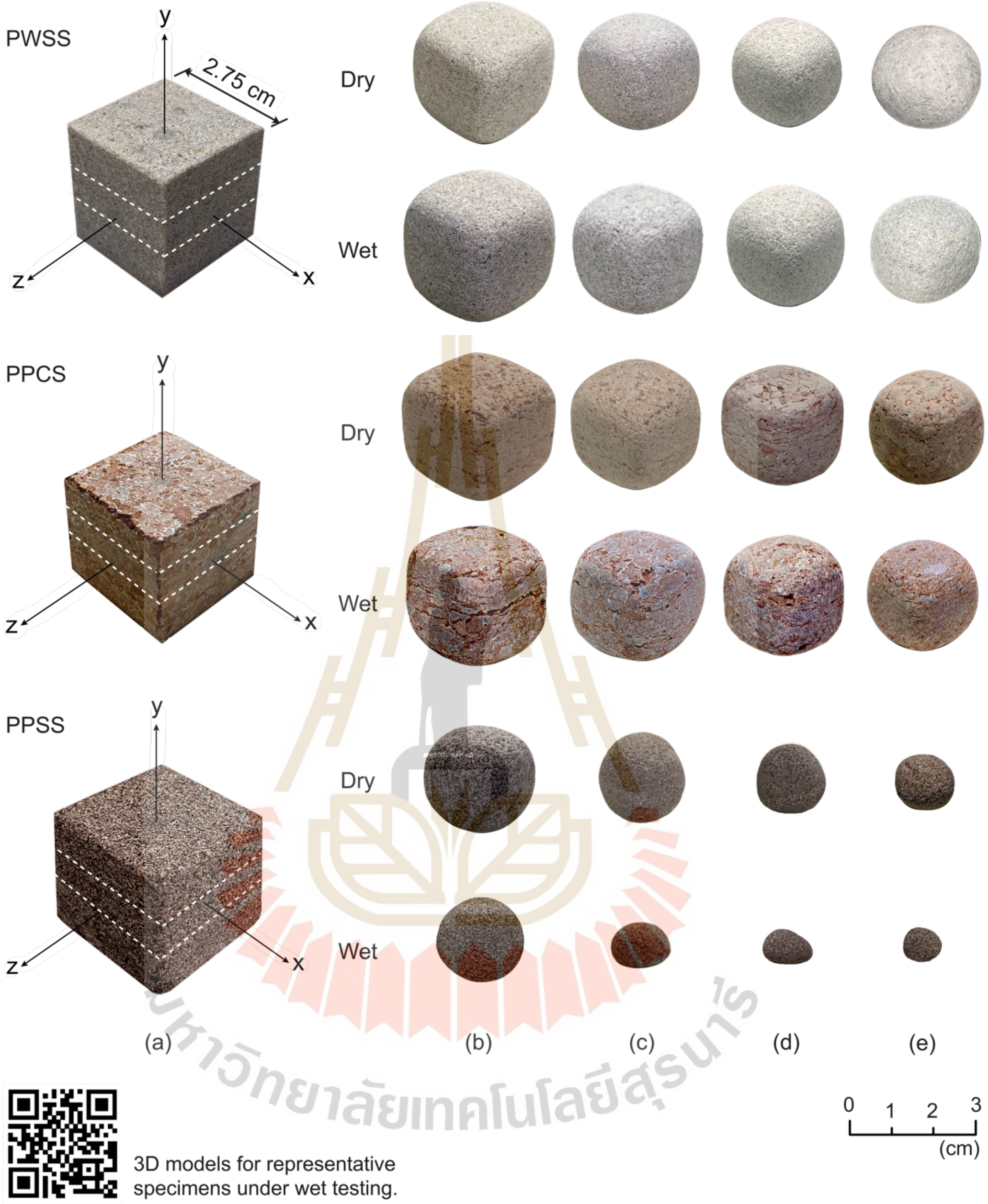

Figure 5.1 Initial cubical specimens (a) and representative images of specimens after subjected to 20 (b), 40 (c), 60 (d) and 80 (e) test cycles.

Roundness (R), sphericity (S), and average size are given in Figure 5.2 through 5.4, respectively. Each rock fragment is determined and classified based on Hryciw et al. (2016), (See Appendix B). Mean and standard deviations of these values after subjecting to 20, 40, 60 and 80 test cycles are summarized in Table 5.1.

According to Figure 5.2, the values of all fragments from the initial condition though 80 test cycles show an increasing of fragment roundness from very angular ($R<0.17$) to different roundness values. After 80 test cycles, PPSS fragments under wet condition can be classified as well rounded ($R>0.7$), while PPCS fragments under dry and wet conditions show only subrounded characteristics ($0.35<R<0.49$). Figure 5.3 plots results with standard deviation of the sphericity values. Except PPSS fragments under wet testing, all rock fragments show linear increases of sphericity values from the initial condition with $S=0.58$ to the test cycle 80 with $S=0.60$-0.67.

The average sizes of ten specimens under dry and wet conditions after subjecting to 20, 40, 60, and 80 cycles are measured based on the narrowest and widest lengths across each side of specimen (detailed in section 4.5). The results are illustrated in Figure 5.4. PPSS specimens under wet tests are decreasing its sizes from 2.95 cm to 0.70 cm within 80 test cycles, which degraded further than those with dry condition and the others under both dry and wet conditions. After test through 80 cycles, the sizes of PWSS and PPCS specimens are slightly deceased with less than 0.50 cm from its initial condition. Excepted for PPCS specimens, the PWSS show a decreasing sizes of fragments under dry testing than those with wet condition.

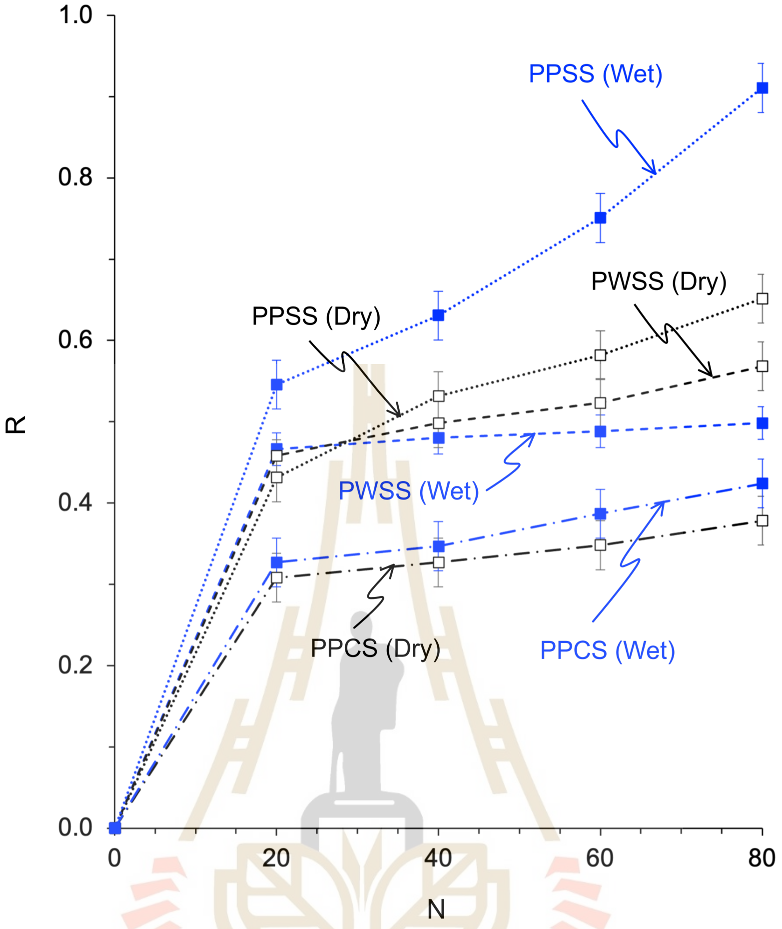

Figure 5.2 Fragment roundness as a function of test cycle (N) measured every 20 days, classified in accordance with Hryciw et. al. (2016). Open points represent dry testing and solid points represent wet testing.

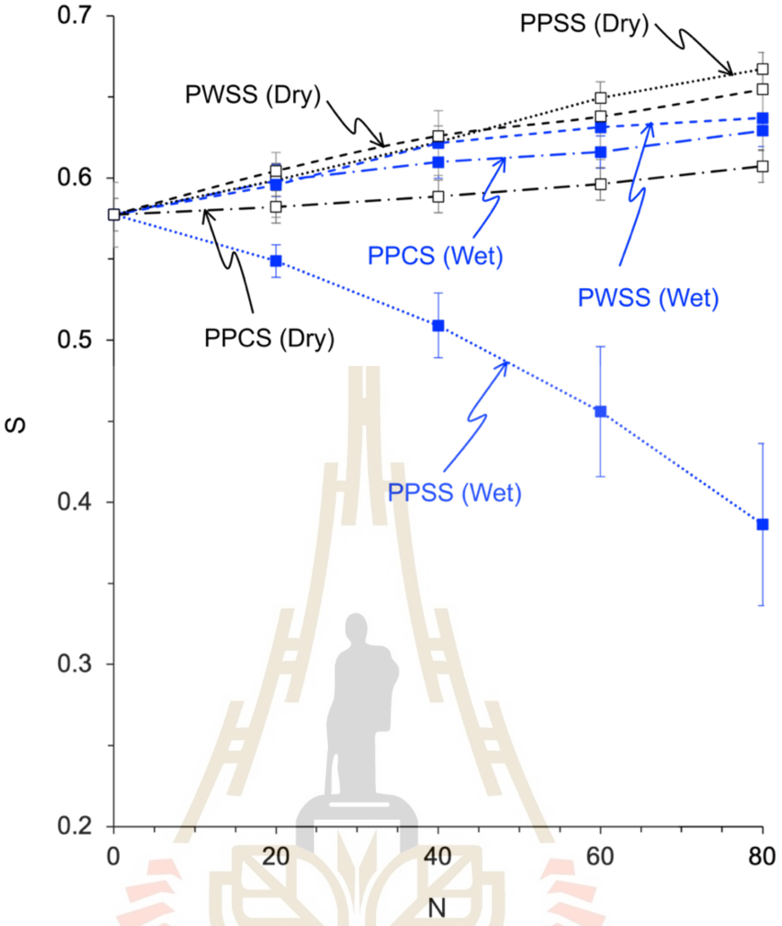

Figure 5.3 Fragment sphericity as a function of test cycle (N) measured every 20 days, classified in accordance with Hryciw et. al. (2016). Open points represent dry testing and solid points represent wet testing.

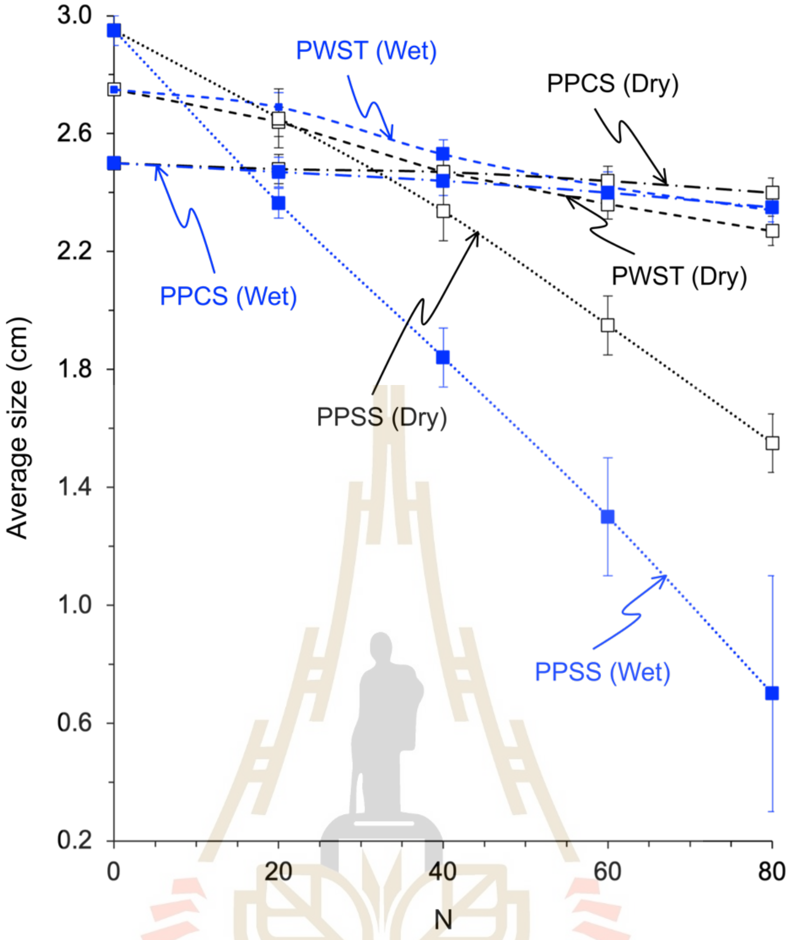

Figure 5.4 Average size of fragments remaining in drum after subjecting under dry and wet tests as a function of test cycle (N). Open points represent dry testing and solid points represent wet testing.

Table 5.1 Mean roundness, sphericity, and average sizes with standard deviation for PWSS, PPCS and PPSS specimens under dry and wet tests.

	N	PWSS		PPCS		PPSS	
Roundness		Dry	Wet	Dry (cm)	Wet	Dry	Wet
	0	-		-		-	
	20	0.46± 0.02	0.47± 0.02	0.31± 0.05	0.33± 0.02	0.43± 0.03	0.55± 0.03
	40	0.50± 0.03	0.48± 0.02	0.33± 0.05	0.35± 0.02	0.53± 0.03	0.63± 0.03
	60	0.52± 0.03	0.49± 0.02	0.35± 0.05	0.39± 0.02	0.58± 0.03	0.75± 0.03
	80	0.57± 0.03	0.50± 0.02	0.38± 0.05	0.42± 0.02	0.65± 0.03	0.91± 0.03
Sphericity	N	PWSS		PPCS		PPSS	
		Dry	Wet	Dry	Wet	Dry (cm)	Wet
	0	0.58		0.58		0.58	
	20	0.60± 0.01	0.60± 0.01	0.58± 0.01	0.60± 0.01	0.60± 0.02	0.55± 0.08
	40	0.62± 0.01	0.63± 0.01	0.59± 0.01	0.61± 0.01	0.62± 0.02	0.51± 0.12
	60	0.63± 0.01	0.64± 0.01	0.60± 0.01	0.62± 0.01	0.65± 0.02	0.45± 0.17
	80	0.64± 0.01	0.65± 0.01	0.61± 0.01	0.63± 0.01	0.67± 0.02	0.39± 0.17
Size (cm)	N	PWSS		PPCS		PPSS	
		Dry	Wet	Dry	Wet	Dry	Wet
	0	2.75		2.50		2.95	
	20	2.64 ± 0.1	2.69 ± 0.1	2.48 ± 0.05	2.47 ± 0.1	2.65 ± 0.1	2.36 ± 0.05
	40	2.47 ± 0.1	2.53 ± 0.1	2.47 ± 0.05	2.44 ± 0.2	2.34 ± 0.1	1.84 ± 0.1
	60	2.36 ± 0.1	2.42 ± 0.1	2.44 ± 0.05	2.40 ± 0.1	1.95 ± 0.1	1.30 ± 0.2
	80	2.27 ± 0.1	2.34 ± 0.1	2.40 ± 0.05	2.35 ± 0.1	1.55 ± 0.1	0.70 ± 0.4

5.2 Passing materials

The passing materials are represented by those smaller than 2 mm (mesh no.10 used for drum openings). As a result from the slake durability test, the weight amount of passing materials obtained from each test cycle is shown in Figure 5.5a through c. For standardized comparison between these results. The passing wight percents from each test cycles are plotted in a semi-log diagram in Figure 5.5d through f. The passing rate is varied with test cycle. The significant reduction of passing materials are suggested from all rock specimens and test conditions. The passing weight percents for PWSS specimens under wet and dry conditions tend to be similar. Both PPCS and PPSS specimens show slightly different percentages of passing materials between wet and dry conditions. The passing of PPSS materials are relatively high within the first 20 cycles. For PPCS specimens, fragments with dry testing tends to show a slightly less of passing materials than those under wet testing.

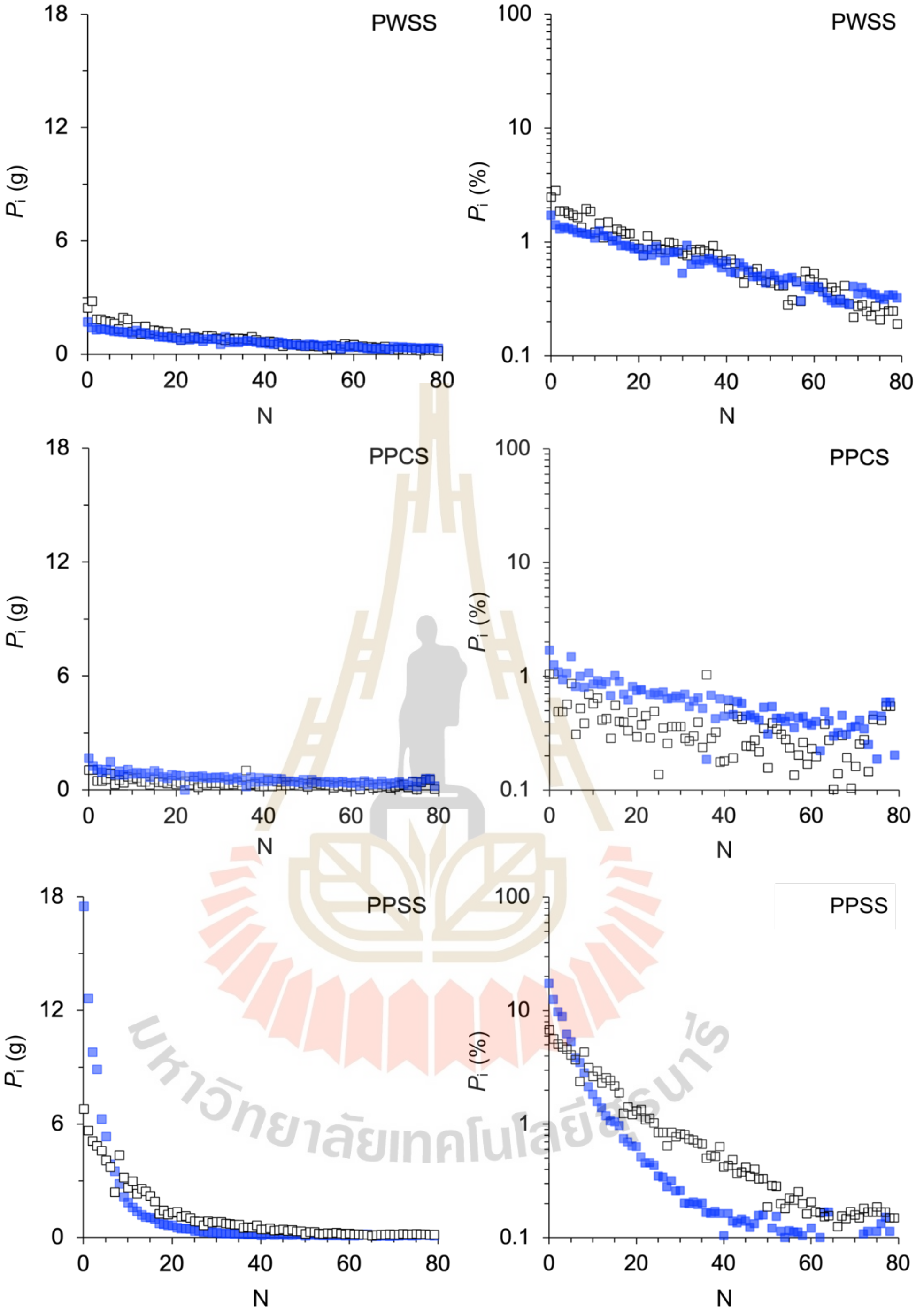

(a) (b)

Figure 5.5 Passing weight (a) and passing weight percent (b), as a function of test cycle (N). Open points represent dry testing and solid points represent wet testing.

5.3 Mineral compositions

X-ray diffraction (XRD) analysis are performed on PWSS, PPCS, and PPSS specimens under initial condition and on those remaining in the drum after 80 cycles of slake durability test. The passing materials of these specimens from test cycle 40 and 80 are also obtained for the analysis. The significant relationship are observed for the compositions of fragments at initial condition and after test cycle 80. Except for those of PPCS specimens that dominantly have calcite minerals, all rock fragments tend to have the same minerals including quartz, feldspars, chlorite, and clays. The weight percent for each mineral is summarized in Table 5.2.

The weight percent obtained from mineral analysis is used for calculation the volumatic percent of each mineral content. The volumatic percent (V_i) for each mineral can be expressed by following equation:

$$V_i = \{\rho \cdot (W_i / 100) / \rho_i\} \cdot 100 \tag{5.1}$$

where V_i is volumatic percent of each mineral (%), W_i is weight percentage of each mineral obtained from XRD analysis (%), ρ_i is density of each mineral (g/cc), i is number of minerals, and ρ is density of fragments (g/cc). Table 5.3 gives the results. Figure 5.6 plots PPCS specimens under dry condition. The volumatic percent of mineral contents are represented as a grouping of feldspars, chlorite, mica, calcite, ferrous oxide, and clay minerals. The results show a slightly decreased proportions on feldspars, chlorite, and ferrous oxide minerals. The significant reduction are spotted on clay minerals. These mineral contents are decreased nearly 6% through the end of 80 test cycles. For PPSS specimens, calcite, feldspars, clay mineral, and mica are observed as a decreasing minerals under wet tests as illustrated in Figure 5.7.

Table 5.2 Mineral compositions in terms of weight percent (W_i) for retained fragments before testing and after 80 test cycles.

			w_i (%)								
Rock types			PWSS			PPCS			PPSS		
Test cycle			Initial	80		Initial	80		Initial	80	
Condition				Dry	Wet		Dry	Wet		Dry	Wet
Mineral composition	Quartz		78.58	84.43	85.09	14.13	15.90	11.10	60.60	67.47	65.37
	Plagioclase		1.99	1.13	1.00	6.81	6.81	6.70	5.93	4.21	2.20
	K-feldspars		3.00	2.71	2.85	2.86	1.87	2.30	0.74	0.57	0.14
	Biotite (Mg-Fe)	Mica	1.89	1.56	1.37	2.31	2.45	2.80	0.26	0.00	0.17
	Muscovite (K)		0.97	0.33	0.27	0.45	0.32	0.39	2.21	2.14	1.08
	illite	Clays	0.64	0.54	0.30	5.36	3.20	4.21	1.30	1.60	2.10
	Kaolinite		5.74	5.32	4.10	2.37	0.44	2.28	1.70	1.20	0.08
	Montmorillonite		0.58	0.27	0.13	0.61	0.08	0.22	0.31	0.07	0.00
	Chlorite		4.32	3.18	4.18	2.01	1.81	1.45	9.22	8.62	14.02
	Calcite		0.23	0.20	0.21	58.28	64.86	62.84	11.32	11.30	8.61
	Dolomite		0.00	0.00	0.00	0.77	0.09	5.21	0.80	0.00	0.00
	Gypsum		0.81	0.23	0.30	1.97	2.10	0.40	2.54	0.00	1.80
	Siderite		0.00	0.00	0.00	0.29	0.07	0.10	0.36	1.56	3.10
	Goethite		0.00	0.00	0.00	0.00	0.00	0.00	0.68	0.43	0.40
	Hematite		0.22	0.10	0.02	1.86	0.70	0.30	1.54	0.83	0.93

Table 5.3 Mineral compositions in terms of volumatic percent (V_i) for retained fragments before testing and after 80 test cycles.

V_i (%)											
Rock types			PWSS			PPCS			PPSS		
Test cycle			Initial	80		Initial	80		Initial	80	
Condition				Dry	Wet		Dry	Wet		Dry	Wet
Mineral composition	Quartz		69.68	73.60	74.49	14.24	15.72	11.02	57.86	58.56	56.00
	Plagioclase		1.77	0.99	0.88	6.87	6.75	6.66	5.67	3.66	1.89
	K-feldspars		2.76	2.45	2.59	2.99	1.92	2.37	0.73	0.51	0.12
	Biotite (Mg-Fe)	Mica	1.53	1.24	1.10	2.13	2.21	2.54	0.23	0.00	0.13
	Muscovite (K)		0.79	0.26	0.22	0.42	0.29	0.36	1.94	1.71	0.85
	illite	Clays	0.55	0.45	0.25	5.20	3.05	4.03	1.20	1.34	1.73
	Kaolinite		5.16	4.70	3.64	2.42	0.44	2.29	1.64	1.06	0.07
	Montmorillonite		0.55	0.25	0.12	0.65	0.08	0.23	0.31	0.06	0.00
	Chlorite		3.74	2.71	3.57	1.98	1.75	1.40	8.59	7.30	11.72
	Calcite		0.20	0.17	0.18	57.42	62.71	60.98	10.57	9.59	7.21
	Dolomite		0.00	0.00	0.00	0.72	0.08	4.81	0.71	0.00	0.00
	Gypsum		0.82	0.23	0.30	2.27	2.37	0.45	2.77	0.00	1.76
	Siderite		0.00	0.00	0.00	0.20	0.05	0.07	0.24	0.93	1.83
	Goethite		0.00	0.00	0.00	0.00	0.00	0.00	0.41	0.24	0.22
	Hematite		0.10	0.05	0.09	0.97	0.36	0.15	0.76	0.37	0.41

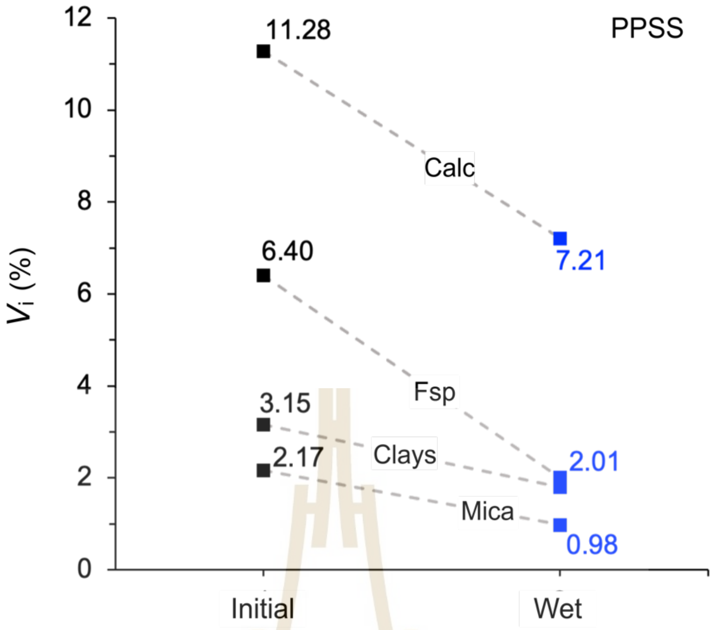

Figure 5.6 Volumatic percent of decreasing minerals for PPSS fragments under wet condition after subjecting to 80 test cycles (Cal=calcite, Fsp=feldspar group, Clays=clay minerals, and Mica=biotite and muscovite)

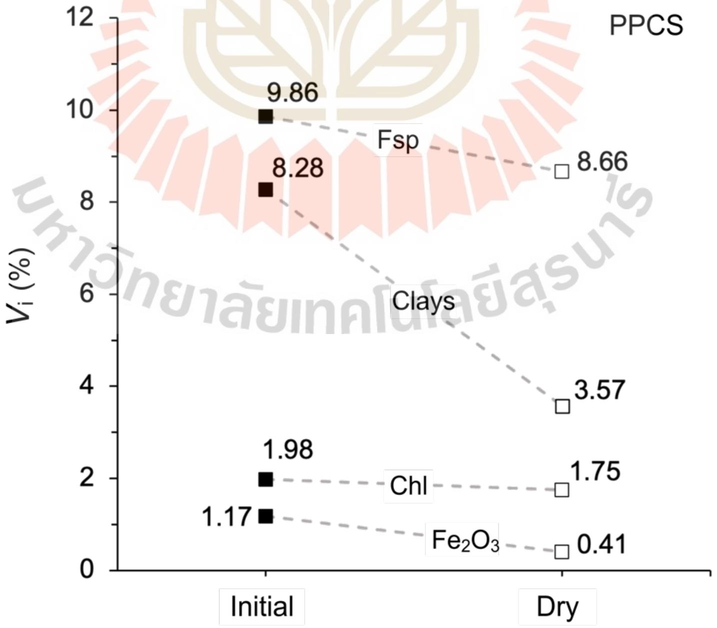

Figure 5.7 Volumatic percent of decreasing minerals for PPCS fragments under dry condition after subjecting to 80 test cycles (Cal=calcite, Fsp=feldspar group, Clays=clay minerals, and Mica=biotite and muscovite).

The results of mineral contents for passing materials of PWSS, PPCS, and PPSS specimens after test cycle 40 and 80 are shown in Table 5.4. The mineral compositions of these particles seem to have a good correlation with the dominant minerals within rock fragments at initial condition. However, the results between test cycle 40 and 80 for all rock fragments are shown that there is no significant relationships. The percentage of dominant minerals are likely having the same amount, which are not correlated with the mineral compositions obtained from the retained fragments after 80 test cycles.

Figure 5.8 plots a peak patterns of each mineral intensity with two theta degrees. The diagrams are illustrated the results of passing materials for PPSS under dry condition from test cycle 40 and 80. The major minerals include quartz, feldspars, chlorite, mica, and clay minerals are observed with a variation of relative two theta. The discrepancy for each mineral content between these test cycles tends to be less than 0.2%.

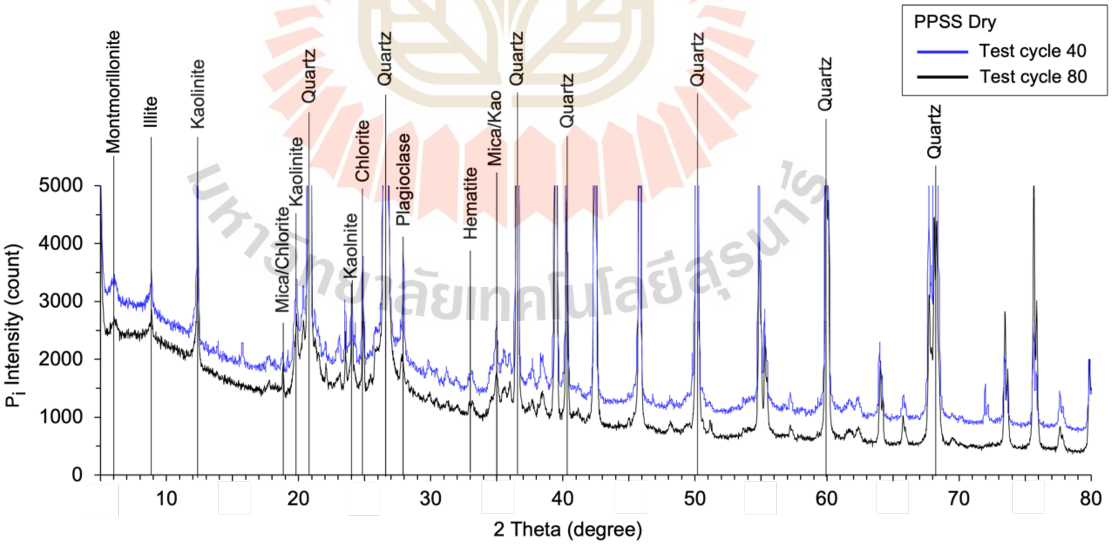

Figure 5.8 Peak patterns of each mineral intensity with two theta degrees of passing materials for PPSS specimens under dry condition after test cycle 40 and 80.

Table 5.4 Mineral compositions in term of weight percent (W_i) for passing materials after 40 and 80 test cycles.

			w_i of passing materials (%)											
Rock types			PWSS				PPCS				PPSS			
Condition			Dry		Wet		Dry		Wet		Dry		Wet	
Test cycle			40	80	40	80	40	80	40	80	40	80	40	80
Mineral composition	Quartz		84.37	85.64	86.63	87.95	13.97	15.81	14.60	14.48	75.18	74.49	73.70	73.65
	Plagioclase		2.12	2.41	2.03	2.55	6.78	6.48	6.97	7.80	3.22	3.72	4.11	3.97
	K-feldspars		2.47	1.99	2.45	2.01	2.87	2.76	2.88	3.04	1.47	0.71	0.99	0.58
	Biotite (Mg-Fe)	Mica	0.55	0.03	0.13	0.11	2.42	0.50	1.38	0.30	0.19	0.29	0.37	0.10
	Muscovite (K)		0.36	0.10	0.19	0.25	0.54	0.22	0.33	0.10	0.96	0.81	0.11	0.62
	illite	Clays	1.17	0.95	1.55	1.22	4.68	6.88	5.82	6.37	4.33	3.10	7.09	6.90
	Kaolinite		3.24	2.49	2.37	2.41	2.14	1.77	1.99	1.67	5.32	4.42	1.50	1.17
	Montmorillonite		0.21	0.10	0.08	0.08	0.63	0.63	0.62	0.61	0.28	0.27	0.53	0.20
	Chlorite		2.64	2.05	2.09	0.76	2.90	1.72	2.46	3.22	1.59	1.66	0.25	1.18
	Calcite		1.32	3.12	0.97	1.61	55.37	55.74	55.95	54.42	2.04	2.13	5.83	7.02
	Dolomite		0.43	0.63	0.55	0.65	3.88	4.73	3.58	4.94	0.69	1.84	0.16	0.70
	Gypsum		0.76	0.39	0.41	0.36	1.80	1.32	1.72	1.78	2.43	3.94	1.56	0.53
	Siderite		0.00	0.00	0.00	0.00	0.32	0.29	0.31	0.33	1.67	1.67	2.41	2.57
	Goethite		0.00	0.00	0.00	0.00	0.00	0.00	0.00	0.00	0.22	0.66	0.78	0.34
	Hematite		0.36	0.10	0.55	0.04	1.70	1.15	1.41	0.94	0.41	0.29	0.61	0.47

5.4 Density

The densities are measured for PWSS, PPCS, and PPSS specimens follow the standard specification of ASTM D7263-21 (detailed in section 4.4). Ten rock fragments under dry and wet conditions after test cycle 20, 40, 60, and 80 are tested. The results of the specimens densities are summarized in Table 5.5. Figure 5.9 plots the results obtained for this study. The diagram shows a reduction trend lines of densities after increasing the test cycles for all rock conditions. PPSS specimens after subjecting to wet tests, their fragments tend to have a significant reduction of density than those under dry testing and the others rocks under both dry and wet testing. The densities from initial condition through 80 test cycles are reducing by 0.26 g/cc for PPSS specimens. However, the fragments of PWSS and PPCS are slightly loss the density after testing through 80 cycles. Excepted for those of rock specimens under dry condition, PWSS specimens show a decreasing of density more than wet tests.

Table 5.5 Densities for PWSS, PPCS and PPSS specimens before testing and after test cycle 20, 40, 60, and 80.

Density (g/CC)	N	PWSS		PPCS		PPSS	
		Dry	Wet	Dry	Wet	Dry	Wet
	0	2.35		2.67		2.53	
	20	2.34	2.35	2.66	2.66	2.47	2.43
	40	2.33	2.34	2.65	2.64	2.38	2.34
	60	2.32	2.33	2.64	2.63	2.33	2.30
	80	2.31	2.32	2.63	2.62	2.30	2.27

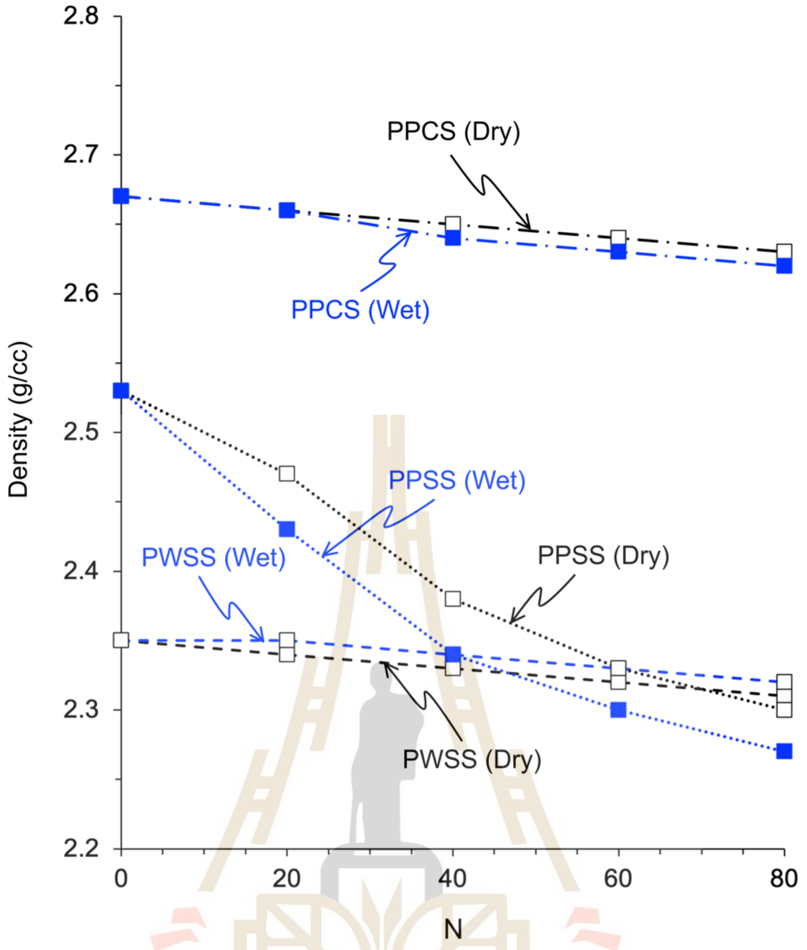

Figure 5.9 Densities of fragments as function of test cycle (N) for PWSS, PPCS, and PPSS specimens after subjecting to 20, 40, 60, and 80 test cycles. Open points represent dry testing and solid points represent wet testing.

CHAPTER VI

TEST RESULTS ANALYSIS

This chapter correlates among the physical properties; shape and size, density, porosity, and mineral compositions for three types of rock specimens under each condition. The analyzation of calculated porosities are also included, based on their mineral volumes before and after test through 80 cycles. The values for calculated porosity are correlated with those obtained from the standard method (ASTM D7263-21). Each condition is analyzed further as the accumulated passing weight percents. The prediction equations from these results can express the estimation of test cycles for fragments to completely disintegrated through the drum, where this parameter can predict the erosive energy for each specimen under different conditions.

6.1 Physical properties

The variation changes of properties for PWSS, PPCS, and PPSS specimens from initial condition through 80 cycles are considered by their physical shape and size, mineral volume, density, and porosity. According to the obtained results, fragments of all test conditions show significantly increase in their roundness and sphericity after subjected to test cycles. Except for those of PPSS fragments under wet testing, the sphericity values are decreased between test cycle 40 and test cycle 80, as their shapes become flatten. However, these fragments are likely shown more roundness when passing though 80 test cycles.

The normalized fragment sizes are calculated. The results are summarized in Table 6.1 and illustrated in Figure 6.1. The reduction of fragments sizes tend to be linear for all test conditions. The PWSS and PPCS fragments are highly durable under both conditions, where less than 20% of their size has been losed after 80 test cycles. Rate of size reduction for PPSS specimens are highest. Their size are losed over 40% after dry testing and nearly 80% are losed after wet testing. Excepted for those of other specimens, PWSS fragments show the significant size reduction under dry testing than under wet testing.

Table 6.1 Normalized fragment sizes for PWSS, PPCS and PPSS specimens before testing and after test cycle 20, 40, 60, and 80.

Normalized size (%)	N	PWSS		PPCS		PPSS	
		Dry	Wet	Dry	Wet	Dry	Wet
	0	100		100		100	
	20	96.00	97.82	99.20	98.80	89.90	80.14
	40	89.82	92.00	98.80	97.60	79.22	62.37
	60	85.82	88.00	97.60	96.00	66.10	44.07
	80	82.55	85.09	96.00	94.00	52.54	23.73

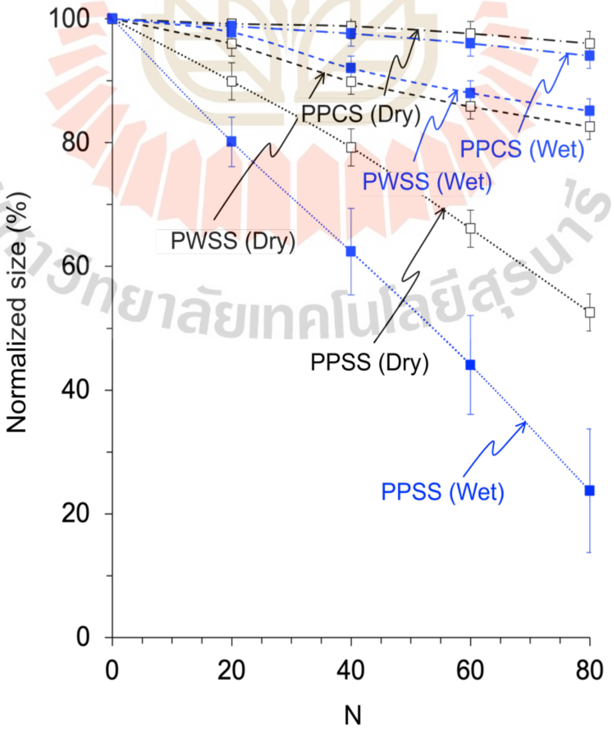

Figure 6.1 Normalized fragment sizes for PWSS, PPCS and PPSS specimens before testing and after test cycle 20, 40, 60, and 80.

The volumatic percent of fragments are correlated with the porosity, as shown in Figure 6.2. The porosities of rock fragments from initial condition through test cycles 80 are analyzed. The calculated porosity is expressed based on Chamwon et al. (2020) as:

$$n_c = \left\{1\text{-}\left[\sum_{i=1}^{n} \rho \cdot (W_i/100)/\rho_i\right]\right\} \cdot 100 \tag{6.1}$$

where n_c represents calculated porosity (%) combining connective and non-connective voids. Porosity of PPSS specimens significantly increased after 80 test cycles, where nearly 15% is obtained under dry testing and 16% under wet testing (Table 6.2). The porosities of PWSS and PPCS specimens remain effectively unchanged from the initial condition through the end of 80 test cycles under both dry and wet conditions. This is reflected by total volumatic percent values of the mineral compositions, as illustrated in Figure 6.2.

The submerging porosity for each specimen is measured follows the standard method, ASTM D7263-21 (ASTM, 2021) comparing with the calculated porosity, where all techniques are measured before and after 80 test cycles. The standard porosity are not measured while testing because of their internal structures that might be loss during subjected to vacuum. The obtained results are shown in Table 6.2. The diagram from Figure 6.3 shows that the calculated porosity seems to be more than that obtained from the submerging method. According to their non-connective voids that the submerging method might take a longer time reaching into the matrix of rock fragments. The results for calculated porosity agree with the fragments density. The normalized densities are analyzed comparing between each rock specimen and condition. Figure 6.4 shows that PWSS and PPCS fragments slightly loss their density less than 2%, where the calculated porosity remained effectively changed only in a few percents after testing through 80 cycles. PPSS fragments under wet testing significantly loss their density more than 10% down to 89.72, where those under dry condition also loss nearly 10% of their density.

Table 6.2 Calculated porosities (n_c) and porosities (n) for PWSS, PPCS and PPSS specimens before testing and after testing through 80 cycles. The n_c is measured with an interval of 20 test cycles.

n_c	N	PWSS		PPCS		PPSS	
		Dry	Wet	Dry	Wet	Dry	Wet
	0	12.35		1.52		6.37	
	80	12.91	12.57	2.22	2.63	14.67	16.05
n	N	PWSS		PPCS		PPSS	
		Dry	Wet	Dry	Wet	Dry	Wet
	0	11.69		1.24		5.17	
	80	12.04	11.76	2.01	2.45	14.53	16.01

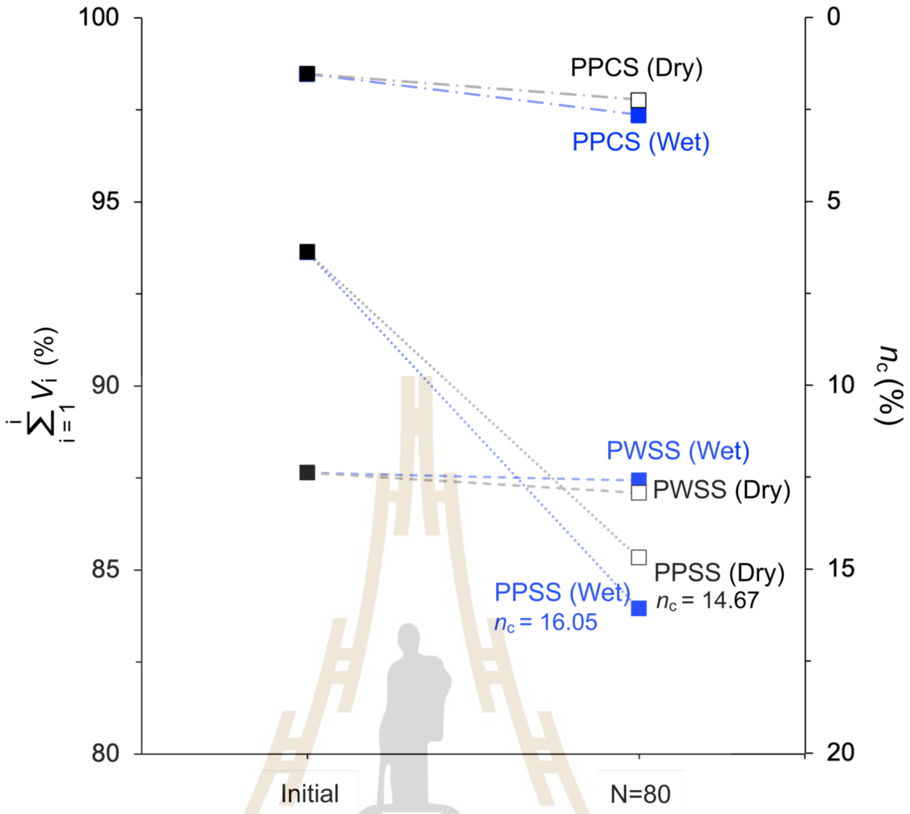

Figure 6.2 Total volumatic percent and calculated porosity (n_c) as function of test cycle (N) for PWSS, PPCS, and PPSS after test through 80 cycles. Open points represent dry testing and solid points represent wet testing.

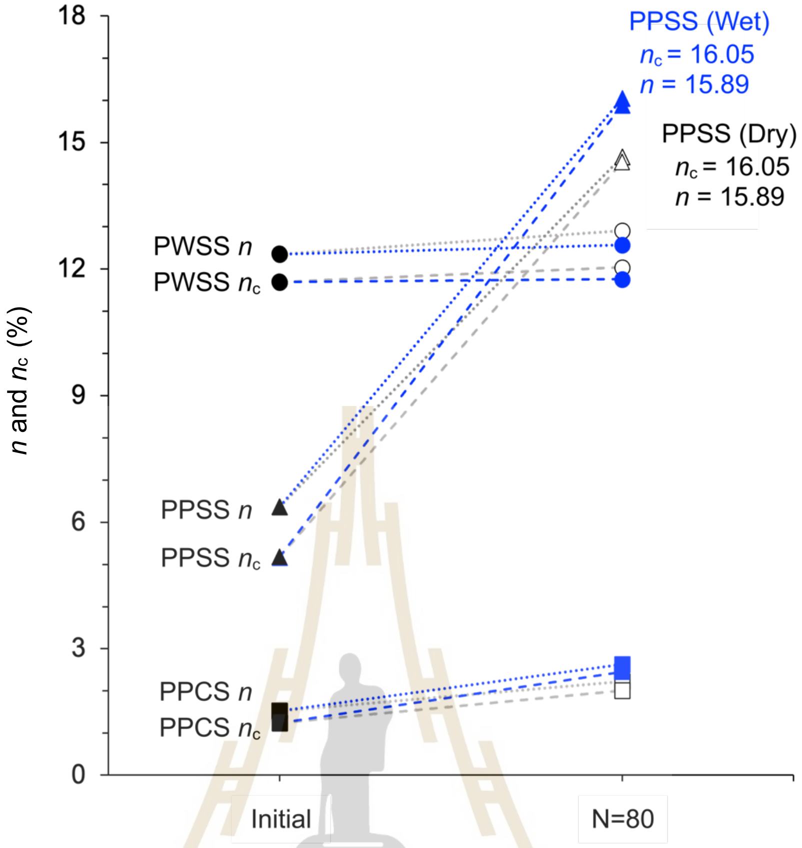

Figure 6.3 Calculated porosities (n_c) compared to submerging porosities (n) for PWSS, PPCS, and PPSS at initial condition and after 80 test cycles. Open points represent dry testing and solid points represent wet testing. Significant increasing of PPSS porosities are shown with the labels.

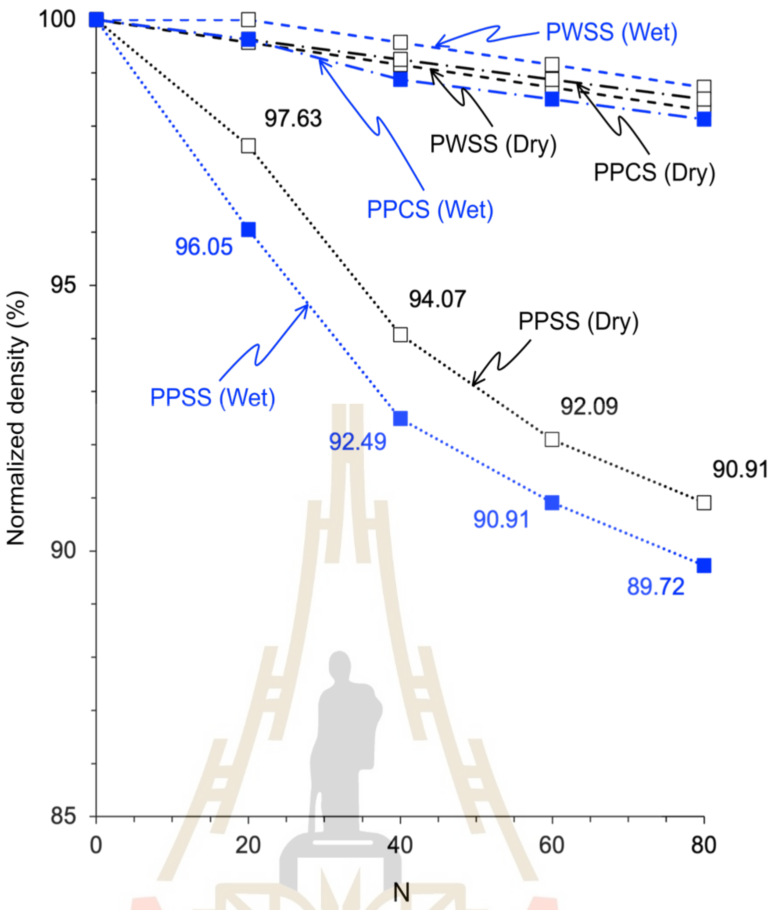

Figure 6.4 Normalized densities as function of test cycle (N) for PWSS, PPCS, and PPSS after subjecting to 20, 40, 60, and 80 test cycles. Open points represent dry testing and solid points represent wet testing. Significant reduction of PPSS densities are shown with the percentage labels.

6.2 Accumulation of passing materials

To clearly show how the specimens from three rock types have passed the drum openings, Figure 6.5 plots accumulated weight percent of passing materials (P_A) from the initial condition through the end of 80 test cycles. Exponential equation is proposed to represent the increase of P_A in a function of test cycle (N) for each test condition and rock specimen:

$$P_A = \alpha \cdot N + [1-\exp(-\delta \cdot N)/\beta] \tag{6.2}$$

where α, β and δ are empirical constants. Their numerical values are given in Figure 6.5. Good correlations are obtained ($R^2>0.9$). According to Figure 5.5b, the passing weight percents for PWSS specimens under wet and dry conditions tend to be similar. Both PPCS and PPSS specimens show slightly different percentages of passing materials between wet and dry conditions. The passing of PPSS fragments are relatively high within the first 20 cycles (up to 10-20%). They rapidly decreased toward 0.2% near test cycle 80. For PPCS specimens, those with dry testing tends to show slightly less passing materials comparing to the wet testing.

Extrapolation of the aforementioned equation to the condition at which all fragments pass through the drum openings (P_A=100%) can predict the number of test cycles needed. The results as summerized in Table 6.3 show that dry and wet testing would require N=219 and 391 for PWSS, 454 and 257 for PPCS, and 135 and 116 for PPSS fragments. These predicted test cycles are later used to calculated the energy required to disintegrate the rocks.

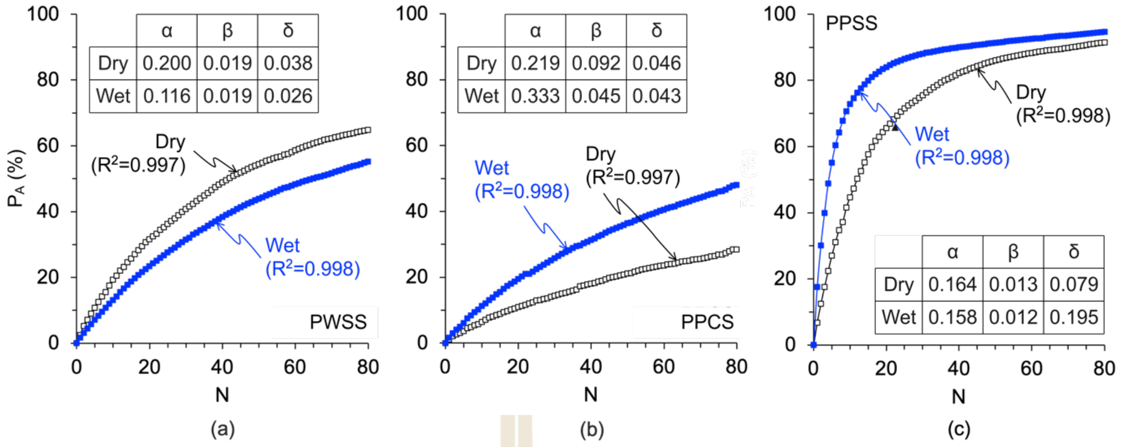

Figure 6.5 Accumulative passing weight percent (P_A) as a function of test cycle (N). Dry testing (open points) and wet testing (solid points). Lines are fitted by $P_A = \alpha \cdot N + [1-\exp(-\delta \cdot N)/\beta]$.

Table 6.3 Test cycle (N) required to obtain 100% passing materials.

Rock type	Condition	N
PWSS	Dry	219
	Wet	391
PPCS	Dry	454
	Wet	257
PPSS	Dry	135
	Wet	116

CHAPTER VII

ENERGY CONSUMPTION

An attempt is made here to determine the energy required to reduce the fragment sizes from the initial condition to be less than 2 mm, i.e., all materials passing through the drum openings. The energy defined in this study relates to the kinetic energy used by rocks during drum rotation. This induces rolling of each fragment, leading to the scrubbing and colliding processes between the fragments and between fragments and inner drum surface (Figure 7.1). Further uses of this energy application are discussed in the following chapter.

7.1 Kinetic energy

On fragment kinetics, the relation of forces reflect their rotating motions with variation of angular velocity depending on rock mass. Rock materials can be losed depending on the amounts of time use for fragments to completely disintegrate their sizes, where less than 2 mm sizes of fragments passing through the drum. The slake durability device forces the rotation of fragments with a constant of acceleration. The device parameters are summarized in Table 7.1. Once testing drums rotate for one revolution, two mechanisms occur: (1) the collision between fragments, and (2) the scrubbing between fragments and drum surface (Figure 7.1). The energy consumed by one rock fragment for one revolution can be calculated as (Meriam & Kraige, 1980a, 1980b):

$$E_{\mathrm{i}} = (1/2)I_{\mathrm{i}} \cdot \omega_{\mathrm{i}}^{2} \tag{7.1}$$

where E_i is rotational kinetic energy (J), I_i is moment of inertia ($kg{\cdot}m^2$), ω_i is angular velocity (rad/s), and i is the number of test cycle (varied from 1 to 80). The moment of inertia is obtained by:

$$I_i = (2/5)m_i \cdot r_i^2 \tag{7.2}$$

where m_i is fragment mass during drum rotation (kg) and r_i is equivalent radius of fragment under dry testing (m).

The masses of rock fragment for each test cycle are different between dry and wet conditions, where the dry fragment mass can be obtained directly from the measurements at the end of each test cycle. For wet testing, the rock fragment is submerged under water in the trough. Its mass (weight) can be obtained by subtracting the dry mass by the buoyancy force (mass of water with the same volume):

$$m_{i,\,wet} = m_i - (V_i \cdot \rho_w) \tag{7.3}$$

where V_i is equivalent volume of fragment at test cycle i (cc) and ρ_w is density of water (g/cc).

The equivalent radius, r_i, can be obtained from the size measurements (Figure 5.4). For example, at initial condition, the equivalent radius is represented by r_0 (i=0) which is equal to 17.37 mm $\{[(28\times28\times28)\cdot(3/4\pi)]^{1/3}\}$. The equivalent volume, V_i, is a representative spherical volume which can be calculated from r_i. Assuming that there is no sliding between fragment surfaces and inner drum surface, the angular velocity of fragment (ω_i) is equal to that of the drum:

$$\omega_i = v_d/r_d \tag{7.4}$$

where v_d is linear velocity of drum (m/s) and r_d is inner drum radius (m). For one drum revolution, the number of fragment revolutions (R_i) at test cycle i can be calculated by:

$$R_i = r_d/r_i \tag{7.5}$$

where r_d is inner drum radius which is constant equal to 0.07 m. As a result, the energy used by a fragment for one drum revolution becomes:

$$E_i = [(1/2)\, I_i \cdot \omega_i] \cdot R_i \tag{7.6}$$

And for one test cycle (2,000 drum revolutions):

$$E_i = [(1/2)\, I_i \cdot \omega_i^2] \cdot R_i \cdot 2{,}000 \tag{7.7}$$

The accumerated energy from test cycles 1 to 80 is

$$E = \sum_{i=1}^{80} E_i \tag{7.8}$$

The energy results are plotted as a function of test cycle in Figure 7.2. The diagrams show that rock fragments tested under wet condition consume energy less than those under dry condition. This is primarily because their submerged weight is about 40% less than their dry weight, and results in a reduction of the moment of inertia. The highest energy is used by dry PPCS specimens (Figure 7.2b) as they have higher density (fragment mass) than the other two sandstones.

Even though the input energy from drum rotation is constant from test cycles 1 to 80, the energy consumed by rock fragments decrease with their sizes, as suggested by non-linear curves of accumulated energy (E) as a function of test cycle (N) in Figure 7.2. Their relation can be best described by a power equation:

$$E = A \cdot \mathrm{N}^{\mathrm{B}} \tag{7.9}$$

where *A* and *B* are empirical constants whose numerical values are given in the figure. The good correlations are obtained (R^2>0.9). Equation (7.9) allows predicting the energy that rock fragments consume to become 2 mm or less. By substituting the numbers of test cycles required to obtain 100% passing given in section 6.3, the energy required for each sandstone type and test condition can be calculated.

The results are given in Table 7.2. Disintegration of dry fragments consumes more kinetic energy than that of water submerged fragments. PPCS specimen shows the highest energy consumption than the other two sanstones. Water penetration decreases its kinetic energy used to reduce the fragment size. The discrepansies of the accumulated energy magnitudes between dry and wet testing reflect the role of water penetration. This explains why the PPCS and PPSS specimens show significant differences in energy consumptions between wet and dry, while the water-insensitive PWSS specimens show comparable energy.

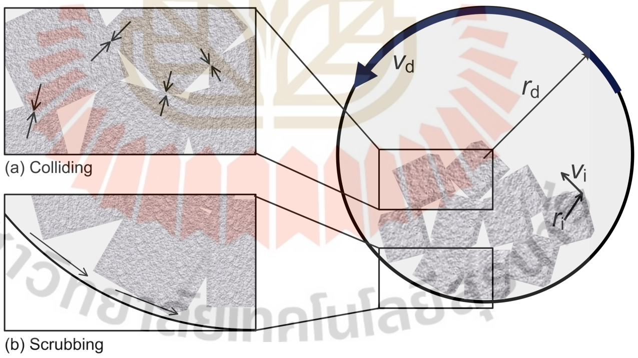

Figure 7.1 Scrubbing and colliding processes between fragments (a) and between fragments and inner drum surface (b).

Table 7.1 Parameters for testing drum.

Parameters	Dimensions	Length (m)	0.10
		Diameter (m)	0.14
	Velocity (m/s)		0.147
	Mass (kg)		0.6

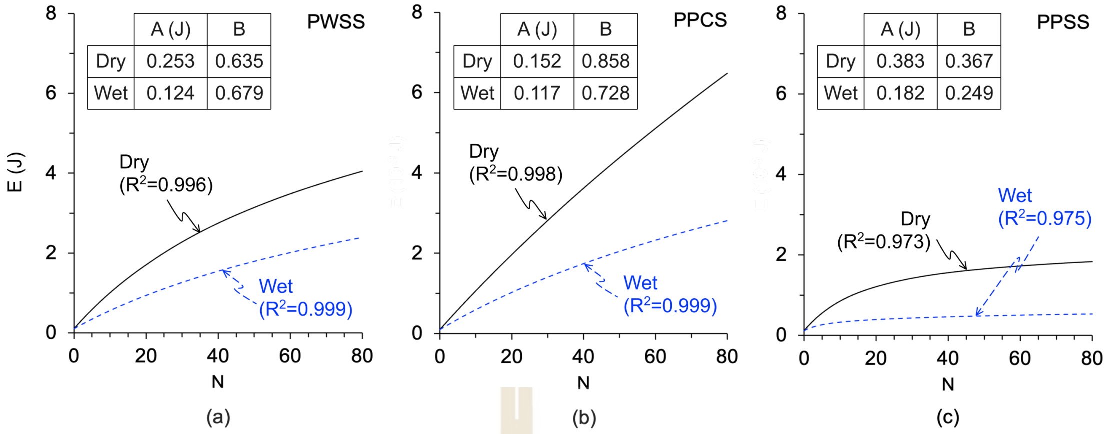

Figure 7.2 Accumulated energy (*E*) as a function of test cycle (N). Dry and wet testing shown as solid lines and dash lines. They are fitted by $E=A \cdot N^B$.

Table 7.2 Prediction of accumulated energy (*E*) and test cycle (*N*) required to obtain 100% passing materials with 2 mm or less.

Rock type	Condition	N	E (J)
PWSS	Dry	219	9.08
	Wet	391	7.14
PPCS	Dry	454	34.02
	Wet	257	9.64
PPSS	Dry	135	2.90
	Wet	116	0.87

7.2 Erosive energy

Figure 7.2 shows the relative of energy for each rock that changed their volumes to the specific sizes. The power equation (7.9) that generally fitted the results through a function of test cycles (Figure 7.2) can transform as a function of equivalent radius, r_i, where each of those values obtained from equation (7.2). The specific energy using for each condition of rocks degraded to interesting radius can be expressed as:

$$E_s = A \cdot e^{rB} \qquad (7.10)$$

where E_s represents the specific energy (J), r_i is the interesting radius (mm), and A and B are the constant parameters as shown in Table 7.3. Good correlations are obtained ($R^2>0.9$). For three rock types, it seem that PPCS specimens under wet condition uses a higher energy than those of others, as the erosive energy tend to increase while having a larger sizes. However, the turning points might be when rocks have a radius around 17 mm, where PPCS specimens continuing with a lower rate of degradation. To specify the amount of energy between two sizes of rocks. The following equation is proposed:

$$E = \int_0^1 (A \cdot e^{Br})\, dr \qquad (7.11)$$

and hence;

$$E = (A/B) \cdot (e^{Br_0} - e^{Br_1}) \qquad (7.12)$$

Figure 7.4 represents only the accumulated energy that has the initial radius of 40 mm. The diagram in Figure 7.4 also are included with the international standards for each fragment from cobbles to sands. The accumulated energy for PPSS specimen with initial radius of 40 mm (cobble size, UCSC) under wet condition disintegrated to the smaller sizes are illustrated in Figure 7.5.

Table 7.3 Constant parameters using in equation (7.10) through (7.12).

Parameters	PWSS		PWCS		PPSS	
	Dry	Wet	Dry	Wet	Dry	Wet
A	$7.69 \cdot 10^{-5}$	$3.63 \cdot 10^{-5}$	$1.24 \cdot 10^{-5}$	$5.96 \cdot 10^{-5}$	$2.06 \cdot 10^{-4}$	$6.10 \cdot 10^{-4}$
B	0.4113	0.4620	0.5185	0.6914	0.3348	0.2467

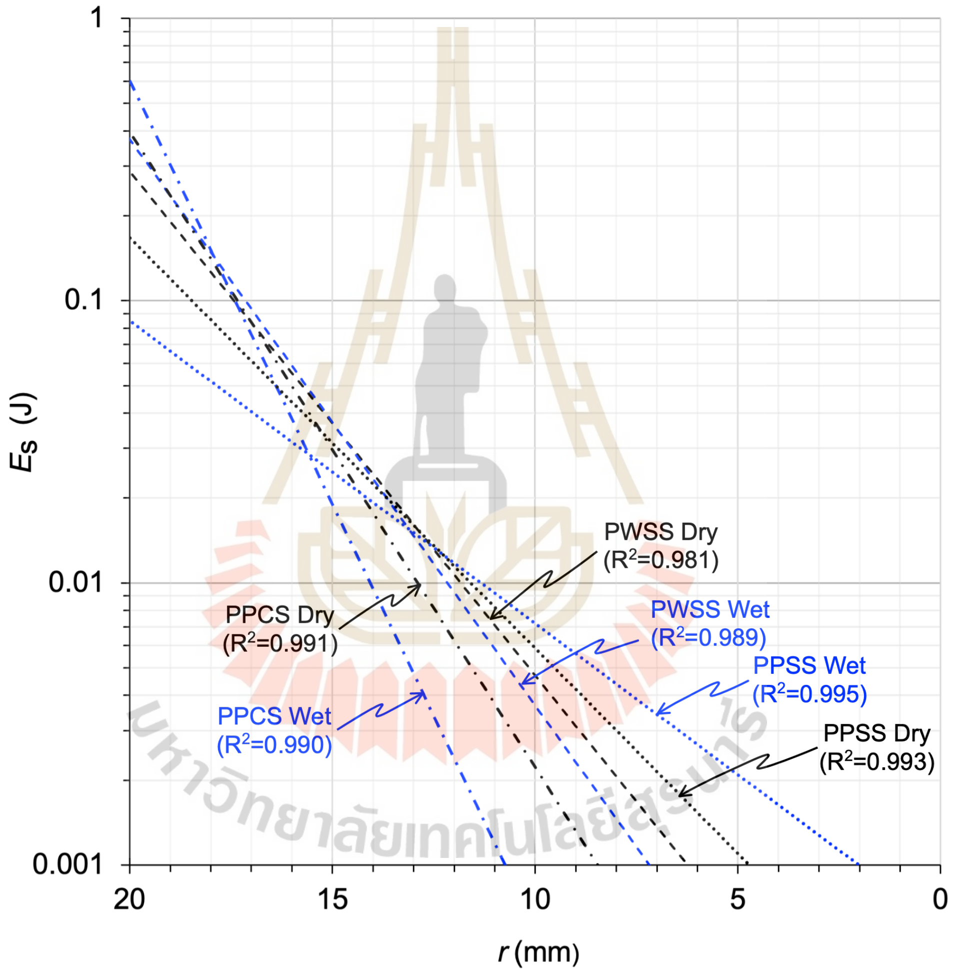

Figure 7.3 Specific energy for PWSS, PPCS and PPSS specimens as a function of equivalent radius (r_i).

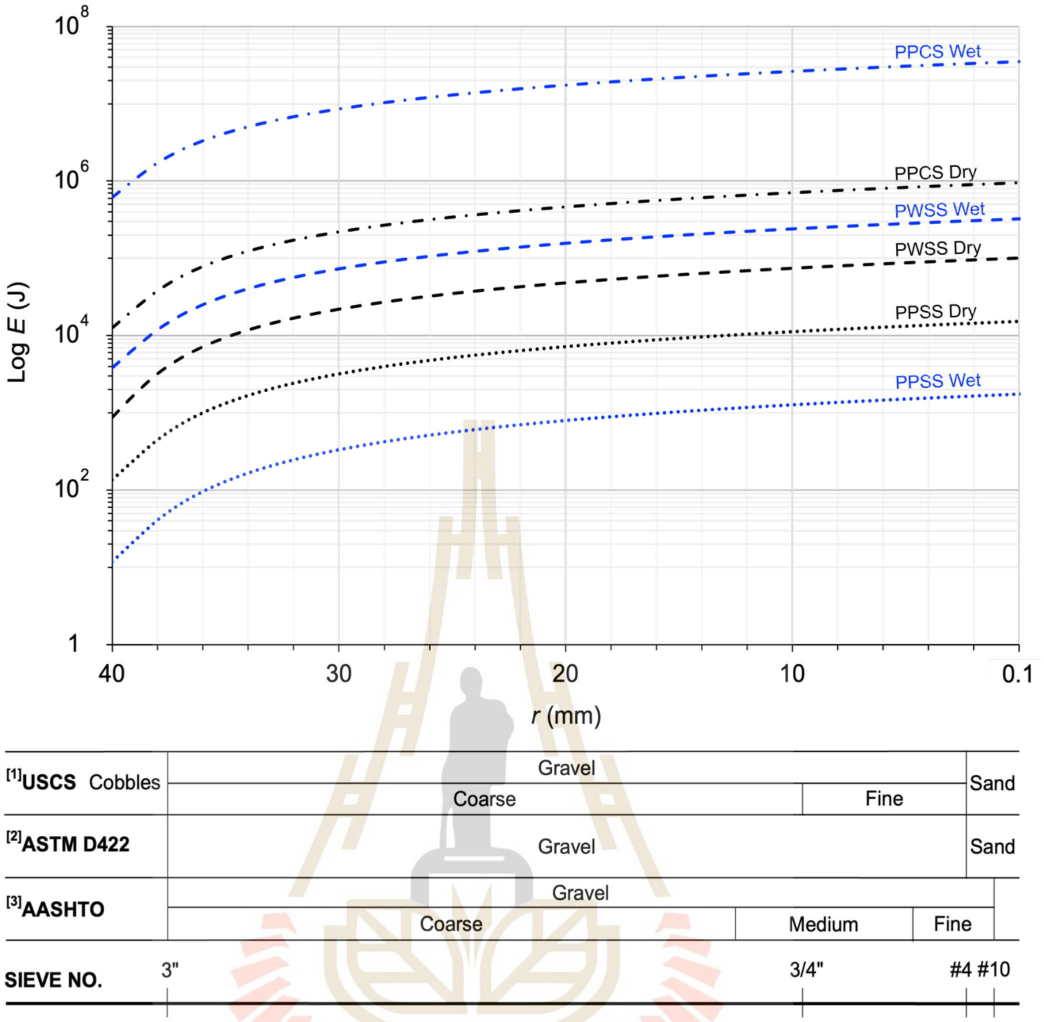

REMARKS:

[1] Unified soil classification system, USCS (ASTM D2487-17)

[2] Particle-size analysis of soils (ASTM D422-16)

[3] American association of state highway and transportation officials, AASHTO

Figure 7.4 Accumulated Energy for PWSS, PPCS, and PPSS specimens with cobbles disintegrated to smaller sizes.

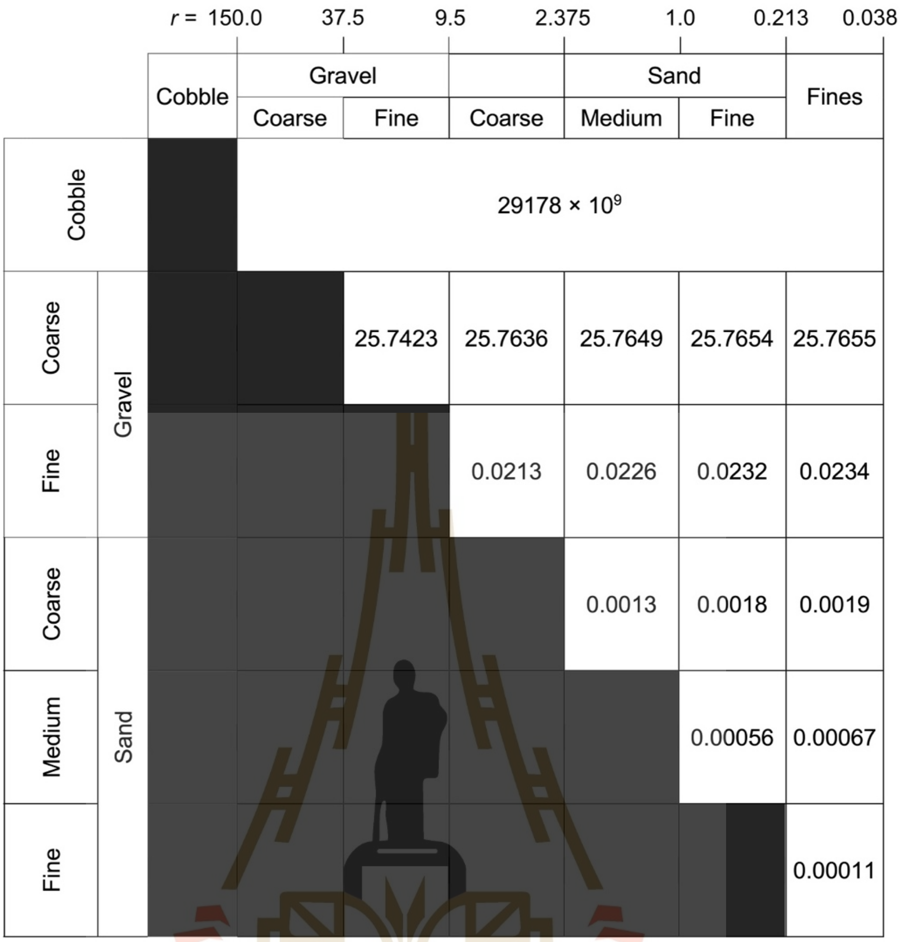

$r =$ 150.0 | 37.5 | 9.5 | 2.375 | 1.0 | 0.213 | 0.038

		Cobble	Gravel			Sand		Fines
			Coarse	Fine	Coarse	Medium	Fine	
Cobble			29178×10^9					
Coarse	Gravel			25.7423	25.7636	25.7649	25.7654	25.7655
Fine					0.0213	0.0226	0.0232	0.0234
Coarse	Sand					0.0013	0.0018	0.0019
Medium							0.00056	0.00067
Fine								0.00011

Figure 7.5 Energy for PPSS specimens under wet condition to disintegrate as a smaller sizes, The classification is followed the unified soil classification system, USCS (ASTM, D2487-17).

CHAPTER VIII

DISCUSSIONS AND CONCLUSIONS

This chapter presents discussions and conclusions of the experimental and analytical studies and recommendation for future study.

8.1 Discussions

Modifications of the slake durability index test parameters of ASTM D4644-16 by increasing the drum revolutions from 200 to 2,000 per test cycle and from 2 to 80 cycles provide a clear trend of deterioration for the three sandstones used in this study. The results not only show different deterioration characteristics among different sandstone types, but also allow deriving mathematical representations to predict the number of test cycles required to completely reduced the rock fragment sizes from 28×28×28 mm^3 (gravel, ASTM D2487-17) to 2 mm (medium sand) or less. Such extreme modifications have never been attempted elsewhere.

As the test cycles progress, Phu Phan bedded sandstone (PPSS) shows higher roundness values and smaller fragment sizes, as compared to those of PPCS conglomeratic and PWSS sandstones, suggesting that it is more susceptible to erosion than the other two sandstones. All sandstone types and test conditions show the increases of sphericity values, except for the PPSS under wet condition. The reduction of PPSS sphericity is probably due to the separation of bedding planes, which occurs more easily when the fragments are in contact with water. This is supported by the fragment images given in Figure 5.1(b), where the larger dimensions are parallel to the bedding planes, and by the fragment size reductions shown in Figure 5.4.

Slaking test induces slightly more deterioration to the PWSS sandstone under dry condition than under wet condition, and results in a higher percentage of passing materials (Figure 6a). This is because scrubbing and colliding effects between fragments are more severe under dry condition. Submersion of the fragments under water in the trough makes them lighter due to their buoyancy forces and reduces fictional resistance between their surfaces. These processes also occur for the PPCS and PPSS sandstones under both test conditions. For these two sandstones, however, water may penetrate into their intergranular boundaries and cementing materials more easily, and subsequently reduce bonding between the grains. The effect of water penetration for PPCS and PPSS sandstones are predominant over the scrubbing and colliding effects, and hence leading to a higher percentage of accumulated passing materials even under wet condition (Figures 6.5b through c). This agrees with the conclusions drawn by Torsangtham et al. (2019) who perform a slake durability testing on the same sandstones in Khorat group.

The mineral compositions of remained fragments are more suitable to correlated with others physical properties than those of passing materials passing through the drums. No distinctive change of mineral compositions of the PWSS and PPCS specimens has been observed from their initial condition to the end of 80 test cycles. This is due to the fact that the slaking test performed here in relatively short-term, and hence chemical alterations are unlikely to occur. Small differences of mineral compositions between their initial and test conditions may be due to the intrinsic variability of the rocks. The water sensitive and soft PPSS sandstone, however, shows notable increases of porosity and reduction of density under both wet and dry conditions (Table 5.3). This is caused by dislodging of feldspar grains and the initiation of micro-cracks and fissures, particularly along bedding planes during slaking test. The easy separation of bedding planes results in relatively flat fragments with lower sphericity values (Figure 5.2).

It is recognized that a variety of sandstone types and textures exists in the northeast of Thailand, only three sandstones have been selected for this study. This is limited by research duration and instrumentation. The presented test series require nearly 500 days (3 sandstones × 2 test conditions × 80 test cycles). The test results, nevertheless, provide a clear trend of erosion behavior for each sandstone type and test condition.

It should be noted that the test results obtained here for the Phu Phan and Phra Wihan formations do not represent the erosion behavior of the entire formations. As reported by Murray et al. (1993), sandstone formations in Khorat group contain a variety of textures, densities, and compositions, depending upon the depth and location.

The porosity determined here is called “calculated porosity” to avoid confusing with the effective porosity as measured by water saturation method specified by ASTM D7263-21. The calculated porosity combined connective and non-connective voids in the rock matrix, while the effective porosity represents only connective voids where they can be penetrated and filled by water.

Even though rock fragments are oven-dried at 105°C for 20 hours for each test cycle, the elevated temperature is excluded from the energy calculation. This is based on the experimental results conducted by several researchers, who conclude that temperatures of less than 200°C have little effect on rock deterioration and mineral alterations, particularly for sandstones (Brotons et al., 2013; Sirdesai et al., 2019; Li & Liu, 2022). Temperature induces thermal expansion to the minerals composing rocks. Sandstones contain mostly quartz and feldspar whose thermal expansion coefficients are similar (Somerton, 1992). For rocks containing minerals with different thermal properties, such as igneous rocks, the effect of elevated temperature becomes significant.

Under in-situ condition the applied kinetic energy to rock fragments can come under different forms, for examples, falling down from hillside, rolling on stream bed by water flow or on desert floor by wind blow, colliding and scrubbing between fragments, and blasting by water or wind-carried particles. For long-term deterioration (e.g. decades or centuries) chemical energy due to weathering, and mineral alteration and thermal energy by repeating heating and cooling cycles would become more significant. Even though the law of energy conservation is valid, the magnitudes and rates of energy consumption to reduce sandstone fragment sizes under in-situ condition would be difficult to predict. In addition, the site-specific environment where the rock fragments are situated, can change from one period to another. The results obtained here, nevertheless, reveal significant findings that the magnitude and rate of kinetic energy consumption by sandstone fragments depend on fragment size, density, porosity, and rock texture. Large fragments can utilize the applied energy more efficiently than smaller ones, as evidenced by the accumulated passing materials in Figure 6.5, and by the energy diagrams in Figure 7.1. Water penetration into fragment matrix helps reducing kinetic energy consumption by weakening the bonding between grains (PPCS specimen) or between bedding planes (PPSS specimen).

8.2 Conclusions

Conclusions drawn from this experimental and analytical investigation can be summarized as follows.

1) Water insensitive PWSS sandstone erodes more quickly under dry condition than under wet condition. Even though it requires longer period to erode under water submersion, due to buoyancy force, it consumes less energy than those under dry condition to reach the same fragment sizes.

2) Sandstone with coarser grains and higher density (e.g. PPCS) tends to be more durable than that with finer grains and lower density (e.g. PWSS), providing that water penetration has insignificant effect during erosion process.

3) For sandstones with comparable mineral compositions as tested here, their erosion characteristics are mainly governed by textures, grain sizes, densities, and structures (bedding planes).

4) Sandstone fragment roundness and sphericity increase as fragment size decreases. The decrease of fragment sphericity can occur during erosion if bonding along bedding planes is weaker that across the beds, particularly when water penetration occurs.

5) Larger fragments use energy more effectively to reduce their size than the smaller ones.

6) The main mechanisms of sandstone erosion under kinetic energy are scrubbing and colliding processes. These physical processes can, however, be predominated by water penetration, depending upon the rock porosity, density, and bonding between grains.

8.3. Recommended for future studies

To understand a more complete erosion behavior of sandstones, more studies are needed as follows:

1) A diverse types of sandstone should be tested. They should have different textures, grain sizes, type of cementing materials and mechanical properties.

2) Long-term deterioration of the rocks under dry and saturated conditions should be integrated, in particular under the consideratives of mineral alterations and their related chemical energy.

3) The long-term testing should also consider the impact of thermal cyclic loading and the thermal energy imposed on the rock fragment.

REFERENCES

ASTM D2487. (2017). Standard practice for classification of soils for engineering purposes (Unified Soil Classification System). *Annual Book of ASTM Standards*. Philadelphia, P.A.

ASTM D4644. (2016). Standard test method for slake durability of shale and similar rocks. *Annual Book of ASTM Standards*. Philadelphia, P.A.

ASTM D7263. (2021). Standard test methods for laboratory determination of density and unit weight of soil specimens. *Annual Book of ASTM Standards*. Philadelphia, P.A.

ASTM E3294. (2022). Standard guide for forensic analysis of geological materials by powder X-Ray diffraction. *Annual Book of ASTM Standards*. Philadelphia, P.A.

Azhar, M. U., Zhou, H., Yang, F., Younis, A., Lu, X., Hou-Guo, F., & Geng, Y. (2020). Water-induced softening behavior of clay-rich sandstone in Lanzhou Water Supply Project, China. *Journal of Rock Mechanics and Geotechnical Engineering*, *12*(3), 557-570.

Brotons, V., Tomas, R., Ivorra, S., & Braga, J. C. (2013). Temperature influence on the physical and mechanical properties of a porous rock: San Julian's calcarenite. *Engineering Geology*, *167*, 117-127.

Chamwon, S., Thongprapha, T., & Fuenkajorn, K. (2020). Correlation between ultrasonic pulse velocities and physical and chemical properties of rocks. *Proceedings of Academicsera International Conference*, 99(1), 46-51.

Charusiri, P., Imsamut, S., Zhonghai, Z., Ampaiwan, T., & Xu, X. (2006). Paleomagnetism of the earliest Cretaceous to early late Cretaceous sandstones, Khorat Group, Northeast Thailand: Implications for tectonic plate movement of the Indochina block. *Gondwana Research*, *9*(3), 310-325.

Corominas, J., Martinez-Bofill, J., & Soler, A. (2014). A textural classification of argillaceous rocks and their durability. *Landslides*, *12*(4), 669-687.

Department of Mineral Resources. (2018). Ministry of Natural Resources and Environment. Bangkok, Thailand.

Dobereiner, L. & Freitas, M.H. (1986). Geotechnical properties of weak sandstone. *Geotechnique*. *36*(1), 79-94.

Erguler, Z. A., & Shakoor, A. (2009). Relative contribution of various climatic processes in disintegration of clay-bearing rocks. *Engineering Geology*, *108*(1-2), 36-42.

Erguler, Z. A., & Ulusay, R. (2009). Assessment of physical disintegration characteristics of clay-bearing rocks: disintegration index test and a new durability classification chart. *Engineering Geology*, *105*(1-2), 11-19.

Fereidooni, D. & Khajevand, R. (2017). Correlations between slake-durability index and engineering properties of some travertine samples under wetting-drying cycles. *Geotechnical and Geological Engineering*. *36*, 1071-1089.

Flores, A. N., Bledsoe, B. P., Cuhaciyan, C. O., & Wohl, E. (2006). Channel-reach morphology dependence on energy, scale, and hydroclimatic processes with implications for prediction using geospatial data. *Water Resources Research*, *42*(6).

Foye, W. G. (1921). Denudation, Erosion, Corrosion and Corrasion. *Science*. *54*(1389), 130-131.

Franklin, J. A. & Chandra, R. (1972). The slake-durability test. *International Journal of Rock Mechanics and Mining Science*. *9*, 325-341.

Fuenkajorn. K. (2011). Experimental assessment of long-term durability of some weak rocks. *Bulletin of Engineering Geology and the Environment*, *70*(2), 203-211.

George, M.F. & Sitar, N. 2012. *Block Theory Application to Scour Assessment of Unlined Rock Spillways*. Technical Report No. UCB GT-12e02. University of California.

Gokceoglu, C., Ulusay R., & Sonmez, H. (2000). Factors affecting the durability of selected weak and clay-bearing rocks from Turkey, with particular emphasis on the influence of the number of drying and wetting cycles. *Engineering Geology*, *57*, 215-237.

Gong, T., Zhu, Y., & Shao, M. (2018). Effect of embedded-rock fragments on slope soil erosion during rainfall events under simulated laboratory conditions. *Journal of Hydrology*, *563*, 811–817.

Goossens, D. (1994). Effect of rock fragments on eolian deposition of atmospheric dust. *CATENA*, *23*(1–2), 167–189.

Gupta, A.S. & Seshagiri, K.R. (2000). Weathering effect on the strength and deformational behavior of crystalline rocks under uniaxial compression state. *Engineering Geology*. *56*(3-4): 257-274.

Hawkins, A. B., & McConnell, B. J. (1992). Sensitivity of sandstone strength and deformability to changes in moisture content. *The Quarterly Journal of Engineering Geology & Hydrogeology*, *25*, 115-130.

Heidari, M., Momeni, A. A., Rafiei, B., Khoodabakhsn, S., & Toorabi-Kaveh, M. (2013). Relationship between petrographic characteristic and the engineering properties of Jurassic sandstones, Hamedan, Iran. *Rock Mechanics and Rock Engineering*, 46, 1091-1101.

Hryciw, R. D., Zheng, J., & Shetler, K. (2016). Particle roundness and sphericity from images of assemblies by chart estimates and computer methods. *Journal of Geotechnical and Geoenvironmental Engineering*, *142*(9).

Inkpen, R. (2007). Interpretation of erosion rates on rock surfaces. *Area*, *39*(1), 31–42.

Jamshidi, A. (2023). Slake durability evaluation of granitic rocks under dry conditions and slaking solution and its prediction using petrographic and strength characteristics. *Bulletin of Engineering Geology and the Environment*, *82*(4).

Keaton, J. R. (2013). Estimating erodible rock durability and geotechnical parameters for SCOUR analysis. *Environmental & Engineering Geoscience*, *19*(4), 319-343.

Kolay, E. & Kayabali, K. (2006). Investigation of the effect of aggregate shape and surface roughness on the slake durability index using the fractal dimension approach. *Engineering Geology*, *86*(4), 271-284.

Koncagul, E. C. & Santi, P. M. (1999). Predicting the unconfined compressive strength of the Breathitt shale using slake durability, Shore hardness and rock structural properties. *International Journal of Rock Mechanics and Mining Science*. *36*, 139-153.

Krautblatter, M., & Moore, J. R. (2014). Rock slope instability and erosion: toward improved process understanding. *Earth Surface Processes and Landforms* , *39*(9), 1273-1278.

Lamb, M. P., Finnegan, N. J., Scheingross, J. S., & Sklar, L. S. (2015). New insights into the mechanics of fluvial bedrock erosion through flume experiments and theory. *Geomorphology*, *244*, 33-55.

Larimer, J. E., Yager, E., Yanites, B. J., & Witsil, A. J. (2021). Flume experiments on the erosive energy of bed load impacts on rough and planar beds. *Journal of Geophysical Research. Earth Surface*, *126*(4).

Lashkaripour, G. R., & Boomeri, M. (2002). The role of mineralogy on durability of weak rocks. *Journal of Applied Sciences*, *2*(6), 698-701.

Li, M. & Liu, X. (2022). Effect of thermal treatment on the physical and mechanical properties of sandstone: insights from experiments and simulations. *Rock Mechanics and Rock Engineering*, *55*(6), 3171-3194.

Li, X., Fu, S., Hu, Y., & Liu, B. (2022). Effects of rock fragment coverage on soil erosion: differ among rock fragment sizes. *CATENA*, *214*.

Lin, M., Jeng, F., Tsai, L. S., & Huang, T. (2005). Wetting weakening of tertiary sandstones-microscopic mechanism. *Environmental Geology*, *48*(2), 265-275.

Lyles, L. (1983). Erosive wind energy distributions and climatic factors for the West. *Journal of Soil and Water Conservation*, *38*(2), 106-109.

Marot, D., Le, V. D., Garnier, J., Thorel, L., & Audrain, P. (2012a). Study of scale effect in an internal erosion mechanism: centrifuge model and energy analysis. *European Journal of Environmental and Civil Engineering*, *16*(1), 1-19.

Marot, D., Le, V. D., Garnier, J., Thorel, L., & Audrain, P. (2012b). Study of scale effect in an internal erosion mechanism: centrifuge model and energy analysis. *European Journal of Environmental and Civil Engineering*, *16*(1), 1-19.

McCarroll, D. & Nesje, A. (1996). ROCK SURFACE ROUGHNESS AS AN INDICATOR OF DEGREE OF ROCK SURFACE WEATHERING. *Earth Surface Processes and Landforms*, *21*(10), 963-977.

McKay, C. P., Molaro, J. L., & Marinova, M. M. (2009). High-frequency rock temperature data from hyper-arid desert environments in the Atacama and the Antarctic Dry Valleys and implications for rock weathering. *Geomorphology*, *110*(3-4), 182-187.

Meriam, J. L. & Kraige, L. G. (1980a). Engineering mechanics volume 1: statics. *Fluid statics* (pp. 306-313). New York, NY: John Wiley & Sons.

Meriam, J. L. & Kraige, L. G. (1980b). Engineering mechanics volume 2: dynamics. *Kinetics of particles* (pp. 460-463). New York, NY: John Wiley & Sons.

Moradian, Z., Ghazvinian, A., Ahmadi, M., & Behnia, M. (2010). Predicting slake durability index of soft sandstone using indirect tests. *International Journal of Rock Mechanics and Mining Sciences*, *47*(4), 666-671.

Moses, C., Robinson, D. A., & Barlow, J. (2014). Methods for measuring rock surface weathering and erosion: a critical review. *Earth-Science Reviews*, *135*, 141-161.

Murray, C., Heggemann, H., Gouadain, J., & Krisadasima, S. (1993). Geological history of the siliciclastic Mesozoic strata of the Khorat Group in the Phu Phan range area, northeastern Thailand. *International Symposium on Biostratigraphy of Mainland Southeast Asia: Facies and Paleontology.* 23-49.

Nichols, G. (2009). *Sedimentology and stratigraphy*. United Kingdom: Willey-Blackwell.

Paripuri, P. S., Parian, M., & Rosenkranz, J. (2020). Breakage process of mineral processing comminution machine - an approach of liberation. *Advanced Powder Technology*, *31*, 3669-3685

Racey, A, Love, .M. A., Canham, A. C., Goodall, J. G. S., Polachan, S., & Jones, P. D. (1996). Stratigraphy and reservoir potential of the mesozoic Khorat group, NE Thailand: Part 1: stratigraphy and sedimentary evolution. *Journal of Petroleum Geology*, *19*(1), 5-40

Scheingross, J. S. & Lamb, M. P. (2017). A Mechanistic Model of Waterfall Plunge Pool Erosion into Bedrock. *Journal of Geophysical Research*, *122*(11), 2079-2104.

Shahid, R. M. (2022). Evaluation of multivariable regression in predicting rock slake durability index. *Scientific Research Publishing House*, *4*(1), 1-20.

Shrestha, D. P. (2008). Guidelines for Monitoring and assessment of wind erosion at site level prepared for Arab center for the study of arid zones and dry lands (ACSAD) damascus, Syria. Retrived from http://www.itc.nl/personal/shrestha /winderosion.pdf.

Sibille, L., Lomine, F., Poullain, P., Sail, Y., & Marot, D. (2014). Internal erosion in granular media: direct numerical simulations and energy interpretation. *Hydrological Processes*, *29*(9), 2149-2163

Sirdesai, N., Mahanta, B., Ranjith, P., & Singh, T. N. (2017). Effects of thermal treatment on physico-morphological properties of Indian fine-grained sandstone. *Bulletin of Engineering Geology and the Environment*, *78*(2), 883-897.

Somerton, W. H. (1992). *Thermal properties and temperature-related behavior of rock/fluid systems* (pp. 148-166). Amsterdam: Elsevier.

Song, H., Jiang, G., Poulton, S. W., Wignall, P. B., Tong, J., Song, H., An, Z., Chu, D., Tian, L., She, Z., & Wang, C. (2017). The onset of widespread marine red beds and the evolution of ferruginous oceans. *Nature Communications*, *8*(1).

Sousa, L. M. O., Surarez del Rio, L. M., & Calleja, L. (2005). Influence of microfractures and porosity on the physico-mechanical properties and weathering of ornamental granites. *Engineering Geology*, *77*(1-2), 53-168.

State Railway of Thailand. 2020. Ministry of Transport. Bangkok, Thailand.

Torabi-Kaveh, M., Mehrnahad, H., Morshedi, S., & Jamshidi, A. (2021). Investigating the durability of weak rocks to forecast their long-term behaviors. *Bulletin of Engineering Geology and the Environment*, *81*(1), 8-30.

Torsangtham, P., Khamrat, S., Thongprapha, T., & Fuenkajorn, K. (2019). Laboratory assessment of long-term durability of some decorating and construction rocks. *Journal of Research and Development*, *30*(3), 135-143.

Trudgill, S. T. 1989, Remeasurement of weathering rates, St. Paul's Cathedral,London. *Earth Surface Processes and Landforms*, *14*, 175-196.

Tugrul, A. and Zarif, L. H. (1998). The influence of mineralogical textural and chemical characteristics on durability of selected sandstones in Istanbul, Turkey. *Bulletin of Engineering Geology and the Environment*, *57*, 185-190.

Veeravinantanakul, A., Kanjanapayont, P., Sangsompong, A., Hasebe, N., & Charusiri, P. (2021). Structure of Phu Phan Range in the Khorat Plateau: Its Apatite Fission Track Ages and Geological Syntheses. *Bulletin of Earth Sciences of Thailand*, *10*(1), 8-16.

Walsri, C., Sriapai, T., Phueakphum, D., & Fuenkajorn, K. (2012). Simulation of sandstone degradation using large-scale slake durability index testing device. *Songklanalarin Journal of Science and Technology*, *34*, 587-596.

Xiang, J., Latham, J., & Pain, C. C. (2022). Numerical simulation of rock erosion performance of a high-speed water jet using an immersed body method. *International Journal of Rock Mechanics and Mining Sciences*, *158*, 105179.

Yan, L., Liu, P., Hua, P., Kasanin-Grubin, M., & Lin, K. (2018). Laboratory study of the effect of temperature difference on the disintegration of redbed softrock. *Physical Geography*, *40*(2), 149-163.

Zhou, Z., Cai, X., Ma, D., Chen, L., Wang, S., & Tan, L. (2019). Dynamic tensile properties of sandstone subjected to wetting and drying cycles. *Construction & Building Materials*, *182*, 215-232.

Zhu, J. J. & Deng, H. (2019). Durability classification of red beds rocks in central Yunnan based on particle size distribution and slaking procedure. *Journal of Mountain Science. 16*(3), 714-724.

Zobeck, T. M., Sterk, G., Funk, R., Rajot, J., Stout, J. E., & Van Pelt, R. S. (2003). Measurement and data analysis methods for field-scale wind erosion studies and model validation. *Earth Surface Processes and Landforms*, *28*(11), 1163-1188